Ripples of Resistance: Unveiling Antimicrobial Resistance Dynamics Along Switzerland's Aare River

Denise Lea Wälchli[1,2], Sasikaladevi Rathinavelu[1], Jane Ackeret[1,3], Norberto Jr Aquino[1,4], Karin Beck[1], David J Janssen[1], Helmut Bürgmann[1, *]

[1]Eawag, Swiss Federal Institute of Aquatic Science and Technology, Kastanienbaum, Switzerland

[2] Department of Plant and Microbial Biology, University of Zurich, Zurich, Switzerland

[3] Department of Environmental Systems Science, ETH Zurich, Zurich, Switzerland

[4] Department of Civil, Environmental and Natural Resources Engineering, Luleå University of Technology, Luleå, Sweden

[*]Corresponding author email contact: helmut.buergmann@eawag.ch

Draft prepared for Submission to *Water Research, 2025-12-12*

Abstract

The global spread of antimicrobial resistance (AMR) is a serious public health concern, driven by widespread antibiotic use and the global environmental circulation of antibiotic-resistant bacteria and resistance genes (ARGs). Wastewater treatment plants (WWTPs) are important sources of anthropogenic AMR entering large rivers, which serve as vital water resources but facilitate downstream dissemination. The drivers and dynamics of AMR propagation along river systems remain poorly understood. As Switzerland's longest and one of its largest rivers, the Aare, situated in the upper Rhine watershed, plays a central role in the 'water castle of Europe'. This study examines the impact of WWTP discharges, some receiving high loads of hospital effluent, on ARG distribution along the 288 km Aare river-continuum. Using quantitative PCR targeting 14 ARGs conferring resistance to eight antibiotic classes, combined with *16S rRNA* gene amplicon sequencing, we conducted a high-resolution spatial survey to assess shifts in the riverine resistome and microbiome. Concentrations of trace metals and nutrients were analyzed as tracers of anthropogenic inputs. Results revealed a progressive increase in ARG abundance downstream, driven by WWTP effluents enriched in ARGs. Effluents had 70-fold higher mean ARG concentrations than upstream waters, raising downstream levels up to 141-fold. Major tributaries such as the Reuss and Limmat sustained elevated ARG levels, while passage through lakes markedly reduced concentrations. This study provides the first detailed baseline for ARG prevalence along a large river system, from pristine headwaters to pollution-affected lower reaches and insights into aquatic AMR dynamics and guidance for future monitoring.

Key words: antibiotic resistance genes, river continuum, wastewater, anthropogenic tracers, quantitative PCR, microbial community

1. Introduction

Bacterial antimicrobial resistance (AMR) has emerged as a major global health and development threat of the 21th century[1]. In 2019, an estimated 4.95 million deaths were associated with AMR, including 1.75 million deaths directly linked to bacterial AMR[1]. According to projections by the UK Government, by 2050 AMR could even be responsible for 10 million deaths, underscoring the urgent need for global action[2,3].

Although antimicrobial resistance genes (ARGs) occur in pristine environments, the levels of resistance observed today are not solely due to naturally occurring resistances, e.g. in antibiotic-producing bacteria[4–7]. Instead, the widespread use of antimicrobials in healthcare and livestock farming has significantly contributed to the spread of antibiotic-resistant bacteria (ARB) and ARGs in ecosystems[8–10]. Human and animal wastes contaminated with antibiotics, ARB and ARGs are continuously released to the environment, either untreated (e.g., agricultural run-off, aquaculture, sewer overflows) or partially treated in wastewater treatment plants (WWTPs). Generally, WWTPs receiving wastewater (WW) from various anthropogenic sources of AMR, including urban areas, hospitals, and specific industries (e.g., pharmaceutical industry and industrial slaughterhouses) are not designed for efficient micropollutant removal or disinfection[11–15]. Consequently, WWTPs have been found to be a major source of ARGs, facilitating their dissemination into aquatic environments[12,16]. While WWTPs quantitatively reduce ARG and ARB loads[17,18], they also serve as hotspots for ARG persistence, horizontal gene transfer (HGT), and bacterial adaption, with effluents exhibiting high transcriptional activity and highly mobilized ARGs[18–20].

Aquatic ecosystems may then contribute to ARG dissemination by acting as a reservoir and conduit of received resistance determinants. This enables acquisition, evolution, and recombination of

57 resistance genes through HGT of mobile genetic elements (MGEs) in pathogenic and clinically
58 relevant bacteria, driving the emergence of new resistance traits[21]. Effluent discharge has well-
59 documented impacts on the resistome of downstream river ecosystems, with ARG primarily
60 persisting in the water column[22,23]. While ARG levels were observed to decrease over short distances
61 (~2 km) from a point source by dilution, and potentially also via sedimentation and degradation, mass
62 balance and fluctuations observed over longer distances (> 10 km) suggest AMR removal, local
63 proliferation and influence of non-point sources on riverine AMR levels[24]. This highlights the role
64 of aquatic environments in the long-term spread and evolution of AMR.

65 Rivers serve as critical interfaces between humans, animals, and the environment. Flowing for
66 hundreds of kilometres, they act as conduits for WW discharge, carrying (micro)pollutants (e.g.,
67 organic chemicals, pharmaceuticals, pesticides, and detergents), as well as ARB and ARGs to
68 downstream ecosystems across landscapes and even continents[11,12,25]. While antibiotics are generally
69 expected to degrade, although at variable rates, the case is less clear for ARB and ARGs[26]. These can
70 decrease through various mechanisms but can potentially also persist for decades[27] or even proliferate
71 under suitable conditions[24]. These contaminants can re-enter the microbiomes of human and animal
72 populations when river water is used for drinking, irrigation, and recreational activities, potentially
73 leading to colonization or in the worst case, causing skin, gastrointestinal, urogenital, and respiratory
74 infections with ARB[28–30].

75 This interconnectedness is of particular importance in Switzerland, often called the "Wasserschloss
76 Europas" (engl. "Water castle of Europe") due to its extensive river networks and vital freshwater
77 resources feeding into major European river systems such as the Rhine, Rhone, and Danube. Swiss
78 rivers shape regional water quality and contribute to the broader European hydrological system,

79 affecting pollution levels in waters across the Swiss border[31]. Protecting these waterways is essential
80 for mitigating the spread of AMR, safeguarding drinking water sources, and maintaining the
81 ecological and public health of large parts of Europe.

82 Previous studies on AMR in larger river systems exposed to strong anthropogenic pressure have
83 mostly targeted heavily polluted sites. While recent research has focused on large European rivers
84 like the Danube[32] and Rhine[33], as well as rivers in China[34–37] and the USA[23,38], no comparable studies
85 were conducted in Switzerland. In general, studies with high-resolution longitudinal sampling and
86 simultaneous examination of potential point sources of contamination are lacking.

87 This study aimed to establish the anthropogenic impact on AMR prevalence along Switzerland's Aare
88 River, from its source to its confluence with the Rhine River. Originating from the Ober- and Unteraar
89 glaciers in the pristine alpine Grimsel region and thus lacking upstream pollution, it flows
90 downstream through increasingly agricultural areas and densely populated cities, where
91 anthropogenic impact increases. We further explored the hypothesis that WWTP effluents in general,
92 and those from WWTP receiving hospital WW in particular, are the primary sources of AMR relative
93 to agricultural sources. Additionally, the study explored potential sinks along the river course,
94 assessing whether AMR is removed, persists, or proliferates. Finally, we investigated whether this
95 system's microbial community structure drives AMR dynamics.

96 **2. Materials and Methods**

97 **2.1. Study area and sample collection**

The Aare, Switzerland's longest river, drains approximately 43% of the country (catchment size: 17'709 km^2) with a mean annual discharge of 555 m^3/s (Gauge Station Siggenthal[39]). The Aare River originates in the high Alps, fed by glacial sources, and flows over 288 km through landscapes characterized by increasing intensity of agricultural and industrial use, population density and urbanization prior to its confluence with the Rhine (**Fig. 1a**). **S1.1** provides a detailed description of the river. Switzerland's temperate climate, with year-round precipitation and distinct seasonal variations, strongly influences discharge, with spring snowmelt being a major contributor.

Field campaign (04 to 14 March 2024) targeted expected low flow conditions prior to snowmelt. In total, 49 samples were collected from the Aare River, its main tributaries and potential contamination sources (**Fig. 1b, Tab. S1**). Effluents of nine municipal WWTP discharging into the Aare River and its tributaries were sampled, seven of which also serve large hospitals (Interlaken, Thun, Bern, Biel, Solothurn, Aarau, and Baden). Two WWTPs (Lyss and Oensingen) receive pre-treated WW from industrial slaughterhouses. At Lyss, an additional sample was collected at the pre-cleaning step. Six tributaries with catchments > 500 km^2 (decreasing catchment size: Reuss > Zihl > Limmat > Saane > Kander > Emme) were sampled near their confluence with the Aare River. Samples downstream of WWTP or tributary inflows were taken 6 – 10 km downstream, where possible, to ensure complete mixing. For samples from the Aare, and points of WWTP discharge and tributary confluence the distance from the source (in river kilometers, rkm) was determined from GPS coordinates of sampling points and a shapefile of the Aare river in QGIS Maidenhead[40].

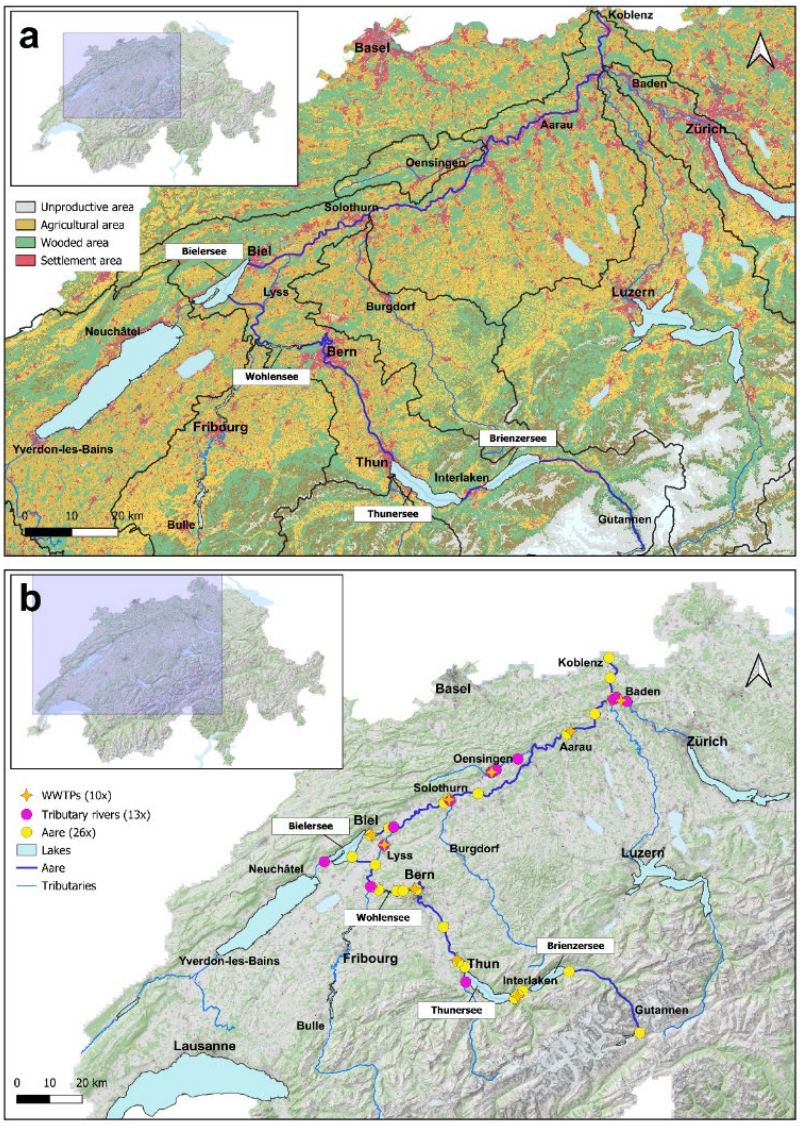

Figure 1: Sampling sites and land use within Aare River's catchment, Switzerland. Lakes are shown in light blue, and the course of the Aare River and its tributaries is indicated in two shades of blue. (a) A zoomed-in version of the Aare catchment, depicting land-use distribution across the Aare and its tributary catchments. Unproductive areas are shown in grey, agricultural areas in yellow, wooded areas in green, and settlement areas in red. (b) Map illustrating 49 sampling locations along the Aare River, the longest river in Switzerland. Sampling includes 10 effluent samples from municipal WWTPs receiving WW from either industrial slaughterhouses (2 samples) or hospitals (8 samples), 26 samples from the main Aare River, and 13 samples from its tributaries (details in Table S1).

127 Samples were primarily collected from bridges to capture mid-river water at ~30 cm depth. A Comet-
128 Combi 12 4T pump (Comet Pumps, Pfefferschwanden, DE) was used. To avoid contamination, the
129 pump, tubing and 5 L plastic sample bottles were rinsed thrice by pumping ~ 5-10 L of river water
130 prior to sampling. Per location 2 x 5 L samples were taken over ~5 minutes for biological analyses
131 except for WWTP effluents (1 x 5 L). Subsamples were obtained for microbial, chemical, and nutrient
132 analysis. A separate grab sample was obtained with a metal-free sampling bucket for trace metal
133 analyses. Metadata (temperature, pH, conductivity, and dissolved oxygen) were recorded in situ using
134 a WTW multi-parameter device, MultiLine 3630 IDS (Fisher Scientific, USA).

135 **2.2 Flow cytometry (FCM)**

136 Total cell count (TCC), and ratios of high nucleic acid (HNA) and low nucleic acid (LNA) cells were
137 determined by FCM on a NovoCyte Advanteon flow cytometer (Agilent, USA) according to the
138 Swiss accredited Standard method 333.1, based on SYBRgreen staining[41]. The procedure followed
139 the methodology described by Proctor and Besmer et al.[42]. Negative controls with sterile-filtered
140 Evian water were included. The gating strategy was recalibrated to ensure accurate differentiation of
141 microbial cells from other particles (see **S1.2, Fig. S1**).

142 **2.3 Biomass Filtration in the Field**

143 Aliquots of all collected water samples were filtered in the field using S-Pak mixed esters of cellulose
144 Membrane filters (GSWG047S6, Millipore, USA) with a pore size of 0.22 µm and a diameter of 47
145 mm. Filters were placed in sterilized polysulfone filter holders (Ref. No. 10461100) with a diameter
146 of 50 mm (Whatman, Germany) under sterile conditions. A peristaltic pump type V6-3L (Shenchen,
147 China) with two pump heads equipped with silicon tubing (# 35 from the manufacturer) was utilized

148 for the filtration process. From each sample, two filter replicates were produced and stored
149 immediately at -20 °C until DNA extraction. Filtration volume (**Tab. S1**) depended on the turbidity
150 of water samples. To avoid contamination between samples, silicon tubing was rinsed with 70%
151 ethanol, followed by nanopure water.

152 **2.4 DNA Extraction**

153 DNA was extracted from both filter replicates using the DNeasy PowerWater Kit (Qiagen, Germany)
154 following the manufacturer's protocol. To optimize yield, the elution volume was reduced to 65 µL
155 per replicate, and the extracts were subsequently pooled, resulting in a final DNA sample volume of
156 130 µL. DNA concentration was quantified using the Qubit 4 Fluorometer (Invitrogen, USA), and
157 purity was assessed with the NanoDrop One spectrophotometer (Thermo Fisher Scientific, USA) (see
158 **Tab. S2**). Blank extractions confirmed that filters and reagents were free of DNA contamination.

159 **2.5 Quantitative PCR (qPCR)**

160 The abundance of a total of fourteen ARGs as indicators for anthropogenic AMR input (*aadA,*
161 *aph(3')-lb*, $bla_{CTX\text{-}M\text{-}1}$, bla_{TEM}, *ermB*, *ermF*, *mcr-1*, *mecA*, *sul1*, *sul2*, *tetA*, *tetM*, *tetW*, *qnrA)* was
162 determined by qPCR. In addition, qPCR was performed for three genetic markers (GM): class 1
163 integron integrase gene *intI1* as a marker for mobile (multi-)resistance cassettes; the beta-
164 glucuronidase gene *uidA* as an *E. coli* specific target to assess fecal contamination, and bacterial
165 *16S rRNA* genes (*16S*) as a proxy for bacterial abundance[43,44]. qPCR assays were performed on a
166 LightCycler®480 (Roche, Switzerland). Standard dilutions (5 x 10^7 to 50 copies/reaction) and
167 negative controls (*no-template*-control: AE buffer; PCR-control: only PCR reagents without the
168 addition of sample) were run in technical quintuplicates, while 1:10 and 1:100 dilutions of each

169 pooled extract and extraction blanks were analyzed in triplicate. Plasmid and synthetic DNA
170 standards were used for calibration. Primer sequences, primer concentration, amount of DNA, and
171 cycling conditions are provided in **S1.3** and **Tab. S3 – S7**. Information on quantification standards
172 is provided in **Tab. S8-S9**. Gene abundances were obtained by normalizing to sample volume,
173 logarithmized (base 10) and reported in units of log copies/L. Calculations for LOD, LOQ, qPCR
174 efficiency, and PCR data analysis, as well as the relative abundance of anthropogenic AMR
175 indicators normalized to *16S* followed the methodology outlined by Rathinavelu et al. and
176 Czekalski et al.[45,46]. qPCR assays met qualitative standards for linearity ($R^2 > 0.99$) and efficiency
177 (90-110%), with the exception of the *tetA* gene ($R^2 = 0.981$) (see **Tab. S7**).

178 For each WWTP location, we calculated AMR contamination potential ($F_{EFF/US}$) and observed
179 WWTP impact ($F_{DS/US}$) as log-transformed ratios of gene abundance (C) in effluent (C_{EFF}) or
180 downstream (C_{DS}) samples, respectively, to the upstream river samples (C_{US}) (**Eq. 1, 2**).

181 $$F_{EFF/US} = \log_{10}(\frac{C_{EFF}}{C_{US}}) \quad \text{(Eq.1)}$$

182 $$F_{DS/US} = \log_{10}(\frac{C_{DS}}{C_{US}}) \quad \text{(Eq. 2)}$$

183 **2.5 *16S rRNA* Gene Amplicon Sequencing**

184 Microbial community composition was assessed by *16S rRNA* gene amplicon sequencing of the V3-
185 V4 region (**S1.4**), performed with PCR-cDNA Barcoding Kit SQK-PCB111.24 on GridION platform
186 using MinION flow cells R9.4.1 (Oxford Nanopore Technologies, UK). Sequencing depth was a
187 minimum of 30,000 reads per sample. Quality control included re-sequencing of samples that showed

matrix inhibition. Resulting FASTQ data were matched against the SILVA database (Release 138, Ref Nr. 99) using EMU[47]. Non-bacterial sequences were removed prior to data analysis.

2.6 Metal, Chemical, and Nutrient Parameters

Total nitrogen (TN) and total organic carbon (TOC) were determined following ISO standards (TN: ISO 11905-1:1998, TOC: ISO 1484:1979) using a Skalar San++ system (Procon AG, Switzerland) and a Shimadzu TOC-L analyzer (Japan). Anions (fluoride, chloride, sulfate) were determined by anion chromatography (930 Compact IC Flex, Metrohm, Switzerland). Dissolved trace metals (Copper (Cu), Zinc (Zn) and Gadolinium (Gd)) and Phosphorus (as total dissolved Phosphorus (TDP) and total Phosphorus (TP) in filtered and unfiltered samples respectively) were quantified by Agilent 8900 ICP-MS equipped with a PrepFAST autosampler, following a protocol adapted from Janssen et al. (2024)[48]. Raw data were processed with MassHunter 5.1 (Agilent). Measurements were conducted in four batches (Sept. 2024 – Apr. 2025) with procedural blanks and a certified reference material (SLRS-6) in each batch (**Tab. S10**). Additional details are provided in **S1.5**.

2.7 Hydrological Data and Total ARG Load

To evaluate discharge dynamics during the campaign weeks from source to estuary, discharge data from nine gauging stations (**Tab. S11**) along the Aare River were obtained from the Swiss Federal Office for the Environment[49]. These data were used to calculate mean daily discharge for each gauge (**Tab. S11**) and then to model sampling point discharge by interpolating between gauging stations and accounting for discharge of major tributaries (**Tab. S11, Fig. S2)**. We then calculated ARG loads (L) for each sampling point in the Aare River and each ARG by multiplying discharge values (Q_i) at each sampling location (i) with ARG abundances according to **Eq. 3.**

209 $L_{ARG}[copies/sec] = Q_i\ [mL/sec] \times C_{i,ARG}\ [copies/mL]$ **(Eq. 3)**

210 Additional discharge and load calculations were conducted for sampling locations in four major
211 tributaries (Saane (rkm 134.8), Emme (rkm 196.5), Reuss (rkm 272.6), and Limmat (rkm 274.1))
212 using data from the gauging station closest to the confluence, and for WWTP effluent discharge using
213 data provided by the WWTP (**Tab. S10, S11**). Predicted ARG gene concentrations downstream of
214 WWTP (C_{DS}) were calculated by applying a discharge-based mixing model using measured WWTP
215 (Q_{WWTP}) and modeled river discharge data ($Q_{US\text{-}River}$) and measured ARG concentrations in US ($C_{US\text{-}River}$)
216 and EFF (C_{WWTP}) (**Eq. 4**).

217 $C_{DS} = (Q_{US\text{-}River} \times C_{US\text{-}River} + Q_{WWTP} \times C_{WWTP}) / (Q_{River} + Q_{WWTP}).$ **(Eq. 4)**

218 **2.8 Data Processing and Visualization**

219 Data handling, statistical analyses and graphics were generated in R[50] using R Studio[51] and the
220 packages ggplot2, cowplot, stringr, scales, grid, readr, knitr, dplyr and tidyr. Species richness and
221 Shannon's alpha diversity index were calculated using the vegan[52] package and differences among
222 groups were tested using the Kruskal-Wallis' test provided in base R. Non-metric multidimensional
223 scaling (NMDS) was performed on *16S rRNA* abundance data with Bray-Curtis distance as the
224 dissimilarity measure (k = 4). Differences in microbial community composition between different
225 waterbodies were tested using PERMANOVA. Spearman rank correlations were performed to assess
226 relationships between microbiological, chemical, nutrient parameters, and concentrations of trace
227 metals. QGIS Maidenhead[40] was used for geographical illustration and map design. Adobe Photoshop
228 was used to fine-tune graphical illustrations.

3. Results

3.1 Background Characterisation of Anthropogenic Influence on the Aare River

Nutrient and metal concentrations show the general anthropogenic impact of urban and agricultural activity along the Aare River. Both TDP (total dissolved phosphorus), representing the bioavailable, short-term reactive fraction, and TP (total phosphorus), reflecting total P-load, remained < 10 µg/L upstream of rkm 118, but concentrations increased further downstream (**Fig. 2c**). WWTP effluents emerged as major point sources, with TP >100 µg/L (except WWTP Thun, 60 µg/L), while tributary P concentrations were generally similar to the Aare River at confluence.

Three trace metals were compared to further characterize anthropogenic impacts: Copper (Cu) and Zinc (Zn) as indicators of diffuse urban, agricultural, and industrial activity[53,54] and gadolinium (Gd) as a specific tracer of healthcare-related inputs[55], reflecting its use as contrast agent in magnetic resonance imaging (MRI). Copper concentrations gradually increased from 0.22 µg/L at the source to 1.07 µg/L at the confluence with the Rhine. WWTPs were point sources with up to 2.6 µg/L Cu (**Fig. 2b**). Zn followed a similar pattern (**Fig. S3**), but in contrast to Cu also increased in the downstream section between Solothurn and Aarau, suggestive of non-point sources such as road runoff and industrial emissions[53]. Gd concentrations showed a similar trend, but with more pronounced increases downstream of WWTPs receiving hospital effluent, notably Interlaken (0.0048 µg/L), Bern (0.04 µg/L), and Aarau (0.03 µg/L). WWTP effluent Gd concentrations were > 0.1 µg/L, 10^1 – 10^2 fold higher than river background. Furthermore, elevated Gd/Cu ratios, especially in Thun, Bern, Biel and Solothurn WWTP effluents, reflect the specific point source input of Gd through WWTP of urban regions with healthcare centres relative to the more varied Cu sources, confirming Gd as a sensitive tracer of healthcare-related discharges (**Fig. S4**).

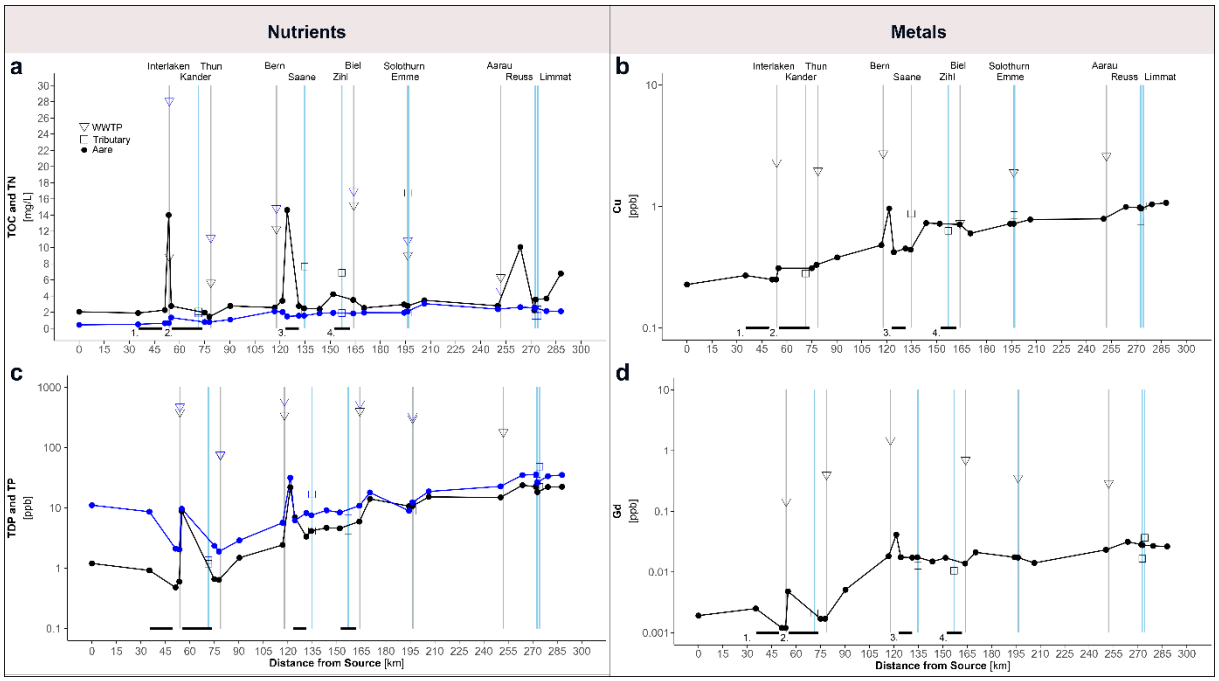

Figure 2: Dynamics of nutrients and metals along the Aare River. Left-side panels show nutrient dynamics: (a) total organic carbon (TOC; black) and total nitrogen (TN; blue), and (c) total dissolved phosphorus (TDP; black) and total phosphorus (TP; blue). Right-sided panels display (b) copper concentrations and (d) gadolinium concentrations. In all panels, values along the river course are shown as continuous lines, while values from WWTP effluents (triangles on grey bars) and tributaries (squares on blue bars) represent input values. Flow-through lakes are indicated as black bars on the x-axis: 1) Brienzersee, 2) Thunersee, 3) Wohlensee, and 4) Bielersee.

3.2 Trends in Microbial Community Abundance and Composition

The observed trends in nutrient and metal distribution are consistent with microbial indicators such as TCC and high HNA fraction, confirming elevated microbial abundance at nutrient-enriched sites (**Fig. 3a, Fig. S5**). TCC values steadily increased roughly ten-fold from the source to the Rhine, ranging from 1.7 x 10^5 to 1.7 x 10^6 cells/mL. Tributaries draining urban areas (e.g., Saane, Reuss, Limmat) showed elevated TCCs, whereas those from more pristine regions (e.g., Emme, Kander) were lower than the Aare at their confluences. *16S rRNA* gene sequencing further revealed clear

266 spatial patterns in microbial diversity and composition (**Fig. 3b, 3c**). Beta diversity analysis using
267 NMDS on Bray-Curtis dissimilarities demonstrated structuring by spatial proximity, with headwater
268 (rkm 0-35) and upper Aare (rkm 35-100) communities being significantly different from more tightly
269 clustered downstream communities (rkm >100) (PERMANOVA: $R^2 = 0.323$, $F = 1.813$, $p = 0.001$,
270 **Fig. 3b**). Tributaries fell into the cluster of the river stretch they entered, except Zihl channel, while
271 composition of WWTP effluent communities was clearly differentiated.

272 These trends in community composition are clearly visible in the phylum level taxon distribution
273 (**Fig. 3c**). Localized shifts in the community were noted e.g., downstream of Thunersee (increase in
274 *Patescibacteria*), around Bielersee (increased *Cyanobacteria*) and in metropolitan areas downstream
275 of WWTPs such as Bern and Aarau, where a notable rise in the abundance of *Firmicutes* and
276 *Campylobacterota* was observed. In WWTP effluents, *Proteobacteria* were consistently dominating,
277 and together with *Bacteroidota* comprising up to 70% of the sequences. *Patescibacteria* were
278 particularly abundant (> 25%) in the WWTP effluents of Thun and Biel and *Firmicutes* were enriched
279 (> 10%) in effluents of WWTPs Interlaken, Thun, Bern, and Biel. In the Aare and its tributaries,
280 considerable variability was observed.

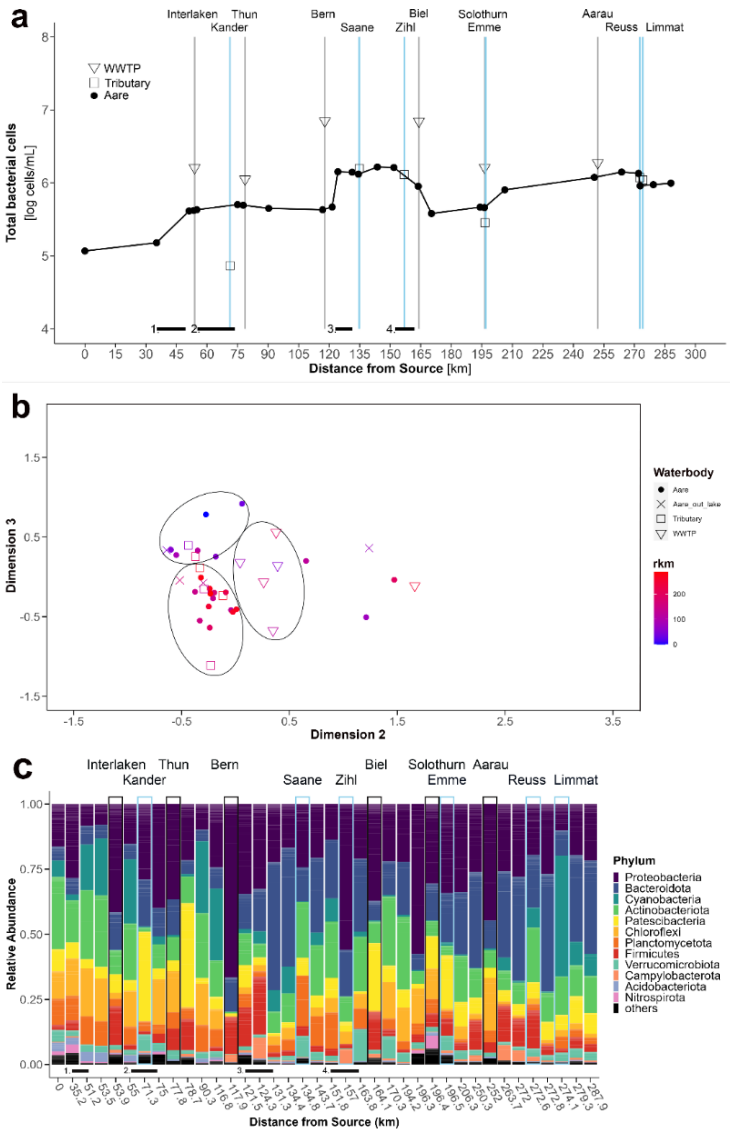

Figure 3: Composition and dynamics of the bacterial community along the Aare River. (a) Total bacterial cell count (TCC) along the river course (black line), including effluents from WWTPs along Aare River (triangles on grey bars), and tributaries (square on blue bars). (b) NMDS ordination showing sample distribution along the Aare River based on community composition, highlighting three aggregates (black circles): i) WWTP effluents, ii) upper reach samples, and iii) lower reach samples. (c) Relative abundance of the 12 most frequent bacterial phyla along the Aare River, its tributaries (blue bars), and WWTP effluents (black bars); remaining phyla are grouped as “others”. Flow-through lakes are indicated as black bars on the x-axis: 1) Brienzersee, 2) Thunersee, 3) Wohlensee, and 4) Bielersee.

291 **3.3 Unique ARG Distribution Patterns Along the Aare River**

292 Out of 14 investigated ARGs, 11 (*aadA*, *aph(3')-lb*, $bla_{CTX\text{-}M\text{-}1}$, bla_{TEM}, *ermB*, *ermF*, *sul1*, *sul2*, *tetA*,
293 *tetM* and *tetW*) were detected in the Aare River (**Fig. 4a**). *qnrA*, *mecA*, and *mcr-1*, which confer
294 resistance to quinolones, methicillin, and colistin, respectively, were not detected in any of the Aare
295 River samples, but *qnrA* was found in two WWTP effluents (**Fig. 4d**). Some ARGs, e.g. those
296 conferring resistance to aminoglycosides (*aadA*), erythromycin (*ermB*), sulfonamides (*sul1*), and
297 tetracycline (*tetW*) were frequently detected and typically the most abundant (**Fig. 4a, Tab. S1**). In
298 contrast, β-lactamase resistance genes ($bla_{\text{CTX-M-1}}$, bla_{TEM}) and the *E. coli* marker gene *uidA* were
299 restricted to low-level detections (< 10^2 copies/mL) at hotspots with high overall ARG
300 concentration (rkm 124 and 250).

301 At the source of Aare River and at rkm 30, ARGs remained undetected, while *16S* was present at
302 ~1.9 x 10^3 copies/mL (**Fig. 4a**). From rkm 45 onwards, *16S* copies increased, consistently
303 exceeding 1 million copies/mL close to the confluence. ARGs and the integron integrase gene *intI1*
304 were first detected at the outflow of Brienzersee near Interlaken, although at relatively low
305 concentrations (10^1 – 10^3 copies/mL) and persisted downstream. *intI1* was highly prevalent along
306 the entire downstream river (up to 10^4 copies/mL) and, with few exceptions, the most abundant
307 AMR indicator. Both absolute (Fig. 4a) and relative ARG abundances (**Fig. S6a**) as well as their
308 total load (i.e. fluxes; **Fig. S7**) increased overall along the river's course. The increase was not
309 continuous, but interrupted by marked local declines in ARG abundance at rkms 75, 130, 165 and
310 marked peaks or increases at rkms 55, 124, 170, 206 until reaching a maximum between rkm 250 to
311 272 (**Fig. 4a**) with ARG diversity broadening in the lower reaches (detections of $bla_{\text{CTX-M-1}}$,
312 bla_{TEM}).

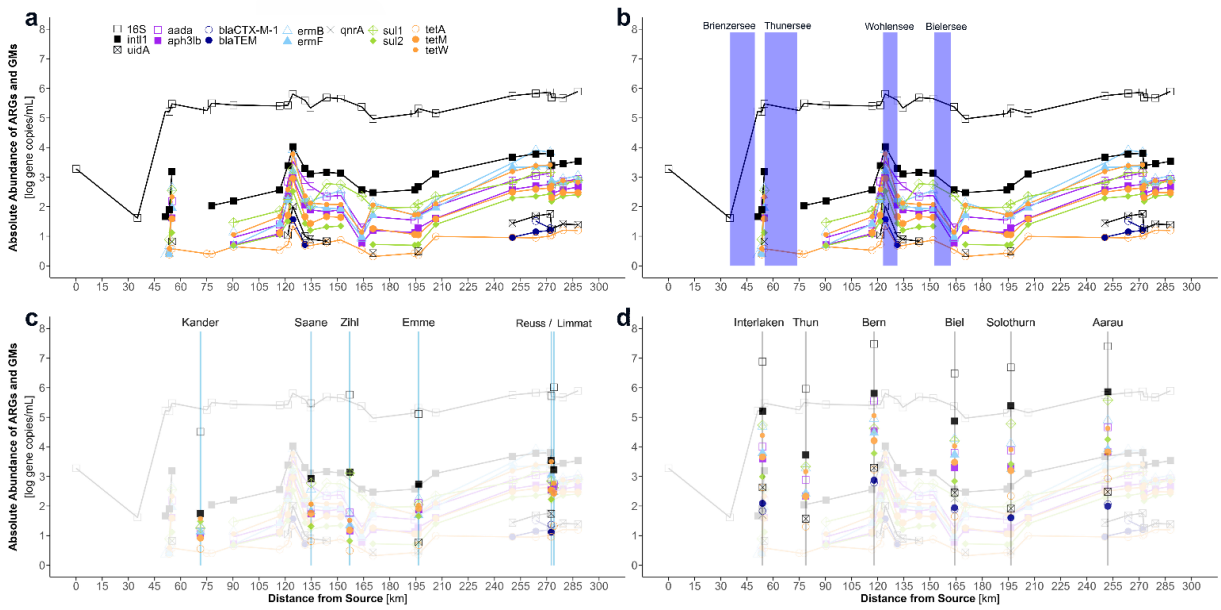

Figure 2: Absolute abundance (log gene copies/mL) of ARGs and GMs, quantified using qPCR. The concentration trends in the Aare River (a) are shown as line plots, while the abundance measured in (c) tributary inflows and (d) WWTP effluents is depicted as symbols within the bars (tributaries: blue / WWTP: gray). Flow-through lakes are indicated as bars in (b). The values are logarithmic - 1 corresponds to 10, and 2 corresponds to 100 copies/mL.

Total load calculations showed that the flux of the *16S* marker gene increased almost 70-fold (5.84 x 10^{12} to 4.06 x 10^{14} copies/sec) while *intI1* increased 1'090-fold (1.63 x 10^{9} to 1.78 x 10^{12} copies/sec) between rkm 51 (ARG detected) and rkm 288 near the confluence. *ermB* increased 7'120-fold (8.1 x 10^{7} to 5.77 x 10^{11} copies/sec), with similar trends for other widespread ARGs, indicating the river's role in downstream ARG transport (**Fig. S7**, **Tab. S12**).

3.4 ARG Patterns of Aare River Shaped by Lakes, Large Tributaries, and WWTPs

Lakes – When ARGs were present upstream of lakes, a pattern of "resetting" ARG abundance was observed when the river passed through a lake (**Fig. 4b**). Thunersee eliminated all ARGs, which had reached a first peak downstream of the city of Interlaken, to levels below detection, with the

328 exception of *tetA*. In contrast, Wohlensee and Bielersee caused a drop in ARG abundance but did
329 not eliminate previously detected ARGs after lake passage, except for *tetM* and *sul2*, which were
330 undetectable for ~7 rkm downstream of the Bielersee outflow. Although no measurements upstream
331 of Lake Neuchâtel were performed, the low ARG abundance in the Zihl canal connecting Lac de
332 Neuchâtel and Bielersee (**Fig. 4c**) is also consistent with this pattern**.**

333 **Tributaries –** Across all sampled tributaries, the same ARGs (*aadA*, *aph(3')-lb*, $bla_{CTX-M-1}$, bla_{TEM},
334 *ermB*, *ermF*, *sul1*, *sul2*, *tetA*, *tetM,* and *tetW*) and GMs (*16S*, *intI1,* and *uidA*) were detected as in the
335 Aare River (**Fig. 4c**). Meanwhile, ARGs *qnrA*, *mecA*, and *mcr-1* remained undetected in all
336 tributaries. A clear positive association of absolute ARG abundance with population density was
337 observed within the catchments, showing tributaries draining larger and more populated areas
338 exhibit higher ARG abundances (Spearman $\rho = 0.89$, $p = 0.033$; **Fig. S8**). Among the tributaries
339 with smaller catchment areas (< 2'000 km^2), the Kander exhibited consistently low concentrations
340 of all markers (< 100 copies/mL), attributed to low population density. In comparison, Saane (1'893
341 km^2) and Emme (976 km^2) rivers, draining more populous regions, showed elevated levels of
342 ARGs, reaching up to 1'000 copies/mL The Limmat River (2'412 km^2) draining the Zurich
343 metropolitan region showed an even higher abundance of ARGs, including *tetA*, which was
344 detected at even higher levels than in the Reuss river (3'426 km^2). The Reuss drains major urban
345 regions in the Cantons Lucerne and Zug, and large parts of central Switzerland, and is the tributary
346 with the largest catchment and overall highest ARG load. At the confluences with Reuss and
347 Limmat, Aare River displayed higher concentrations of both ARGs and GMs compared to the
348 inflowing tributaries, which resulted in a dilution effect downstream of the confluence (**Fig. 4c**).

349 **Wastewater –** WWTP effluents consistently contained high ARG abundances exceeding those in
350 river water (**Fig. 4d**). In addition to *uidA* and *intI1*, 9 out of 14 ARGs were detected across all
351 effluents, including genes conferring resistance to aminoglycosides (*aadA*, *aph(3')-lb*, sulfanomides
352 (*sul1*, *sul2*), tetracyclines (*tetA*, *tetM*, *tetW*), and macrolides (*ermB*, *ermF*). bla_{TEM} was absent only
353 in WWTP Thun, while $bla_{\text{CTX-M-1}}$ was found only in effluents from WWTPs Interlaken, Bern, Biel,
354 and Aarau. *qnrA* appeared at low levels (50 – 180 copies/mL) in WWTP Interlaken and Biel. *mcr-1*
355 and *mecA* were not detected.

356 The observed contamination downstream of WWTP (log DS/US ARG abundance ratio; $F_{EFF/US}$, **Fig.**
357 **5a**) mirrored the WWTP contamination potential (log EFF/US ARG abundance ratio, $F_{DS/US}$, **Fig. 5b**).
358 Inflows of WWTP effluents, with on average 70-fold (geometric mean; average $F_{DS/US}$: 1.9) higher
359 ARG concentrations than upstream river water ($F_{DS/US}$ range: -0.2 to 4.2, **Fig. 5b**) led to 4-fold (0.6
360 log) downstream increases of ARGs in the receiving river ($F_{DS/US}$ range: -0.4 to 2.1, **Fig. 5a**). Negative
361 $F_{DS/US}$, indicating ARG abundance at or below background levels, were only observed for the
362 effluents of the pre-clean stage of the slaughterhouse at Lyss and the smallest WWTP, Baden.

363 The contamination potential (log EFF/US ratio, $F_{EFF/US}$) of the effluent was similar for all genes, the
364 Kruskal-Wallis test ($p = 0.489$) and pairwise Wilcoxon comparisons found no statistically significant
365 difference between genes (**Fig. 5b**). The large WWTP in Bern (design capacity > 300 kPE), which
366 also receives WW from the Inselspital (University Hospital) had the highest ARG contamination potential
367 with a median $F_{EFF/US}$ of 3.1. The small WWTP of Lyss (pre-clean, <30 kPE, $F_{EFF/US}$ =0.53) and Baden
368 (<50 kPE, $F_{EFF/US}$ =0.71) also had the lowest ARG contamination potential. However, no significant
369 relationship ($R^2 = 0.14$, $p = 0.29$) was observed between ARG contamination potential and design
370 capacity overall (**Fig. S9**).

371 Comparing $F_{DS/US}$, Kruskal-Wallis test ($p = 0.223$) and Wilcoxon pairwise tests again showed no
372 significant difference between genes. WWTP impact varied by site (**Fig. 5a**). The strongest median
373 contamination impact (1.66) was observed at WWTP Bern (> 300 kPE). The increase was
374 particularly high for *aadA* (141-fold), *aph(3')-lb* (75-fold), *tetW* (132-fold), *tetM* (68-fold), and
375 *ermF* (61-fold). No impact (i.e. negative $F_{DS/US}$) was observed more frequently (n=14) than for
376 contamination potential, mainly at WWTP Baden, Oensingen and Biel.

377 Applying a discharge-based mixing model, the expected downstream ARG concentration matched
378 observations closely ($R^2 = 0.88$, $p = 0.005$, m=0.80, **Fig. S10**), confirming that the observed
379 increases are due to the WWTP effluent. The impact of WWTP of urban centers thus consistently
380 resulted in a marked increase in ARG concentrations, loading, and relative abundance in the Aare
381 River. This is most pronounced downstream of WWTP Interlaken and Bern (**Fig. 4a, d**) but is also
382 contributing to the cumulative increases downstream of Biel (rkm 164-170), Solothurn (rkm 196-
383 206), and up to Aarau (rkm 206-272).

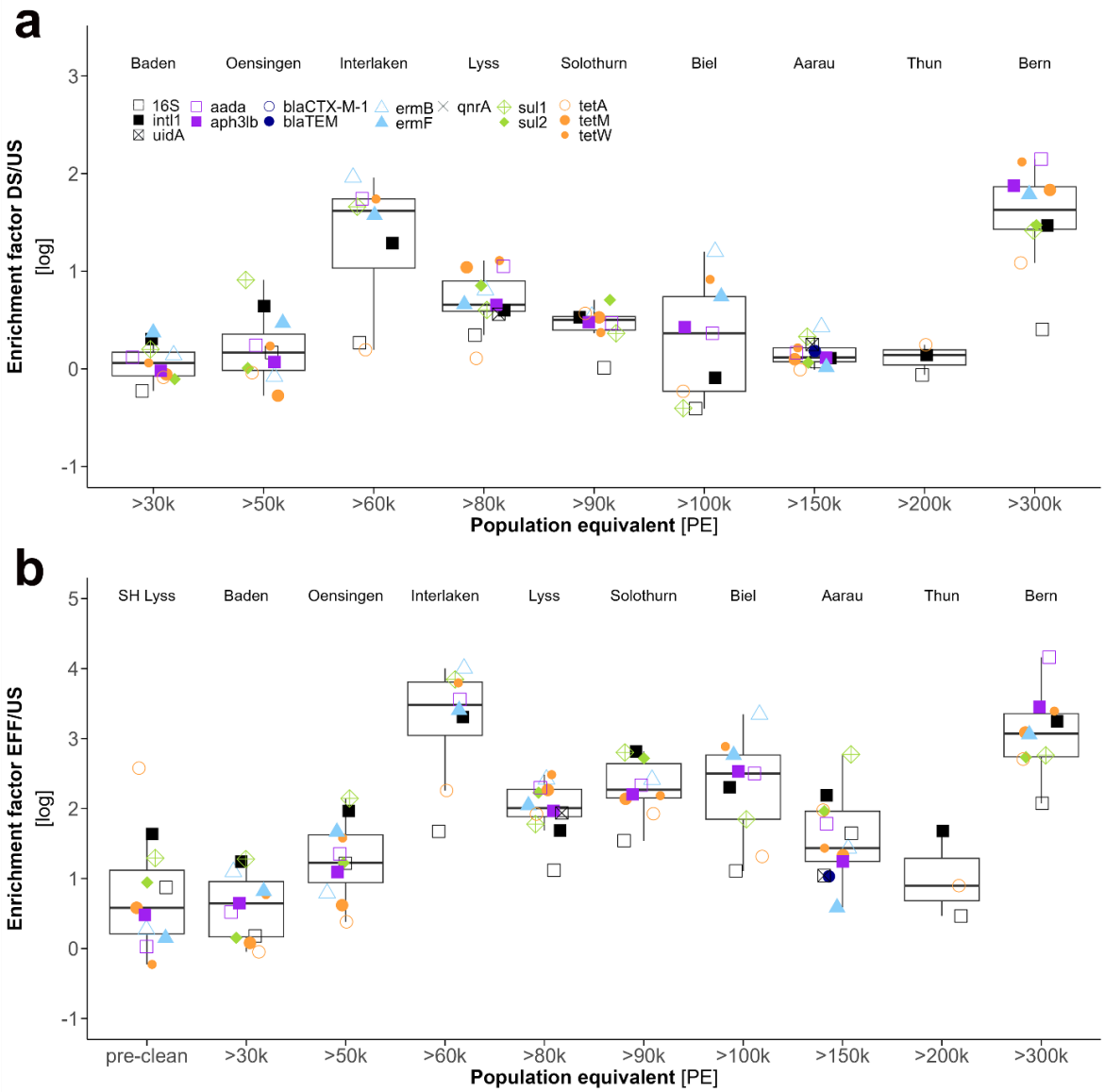

Figure 5: Observed contamination (DS to US ratio) and contamination potential (EFF/US ratio) of the absolute abundance of ARGs and GMs with increasing design capacity (PE) of WWTPs. For evaluation of contamination potential and the impact of WWTP effluent on ARG and GM abundance in receiving river, log10-transformed ratios of ARG abundance were calculated for (a) downstream relative to upstream, and (b) WWTP effluent relative to the upstream river. Results were ordered by the design capacity (population equivalent, PE) of WWTPs. Three WWTPs located on tributaries of the Aare river were also included: Baden (Limmat), Lyss (Alte Aare), and Oensingen (Dünnern). The latter two receive wastewater from slaughterhouses in addition to communal wastewater.

394 **3.6 Correlation between ARG and other indicators of anthropogenic impact**

395 To identify factors associated with variations in the abundance of ARGs and microbial marker genes
396 (*intI1*, *16S* and *uidA*), we calculated Spearman rank correlations with microbiological and chemical
397 parameters and concentrations of nutrient and trace metals. Correlation analyses were performed
398 separately on samples collected i) along the Aare River (**Fig. 6**) and ii) on effluents from 10 WWTPs
399 along the Aare River and its tributaries (**Fig. S11**). To capture spatial trends along the river continuum,
400 "km from source" (distance) was included as a parameter.

401 In river water samples, we observed mostly positive correlations between parameters, with the
402 exception of fluoride, sulfate, pH, DOC, and LNA abundance (**Fig. 6**). Distance emerged as a strong
403 predictor of most parameters, including ARG abundance. Strong positive correlations ($\rho > 0.7$) were
404 observed between distance and the abundance of *aph(3')-lb*, *ermB*, *intI1*, *sul1*, *sul2*, *tetA*, and *tetW*
405 but also TP, TDP, chloride, nitrate, and TN ($\rho > 0.8$). Trace metals, particularly Cu, also increased
406 with distance.

407 Across the dataset, most ARGs showed highest correlation coefficients with one another ($\rho > 0.85$),
408 except for *β*-lactamase genes ($bla_{CTX\text{-}M\text{-}1}$ and bla_{TEM}), which displayed only moderate correlations with
409 other ARGs ($\rho = 0.4$–0.7) but co-occurred strongly with each other ($\rho > 0.8$). *16S, TCC* and *uidA*
410 abundances correlated with ARG occurrence, supporting their roles as indicators of total bacterial
411 load and faecal contamination. Notably, Gd correlated highly with nearly all ARGs ($\rho > 0.65$), with
412 the rare β-lactamases being the only exception.

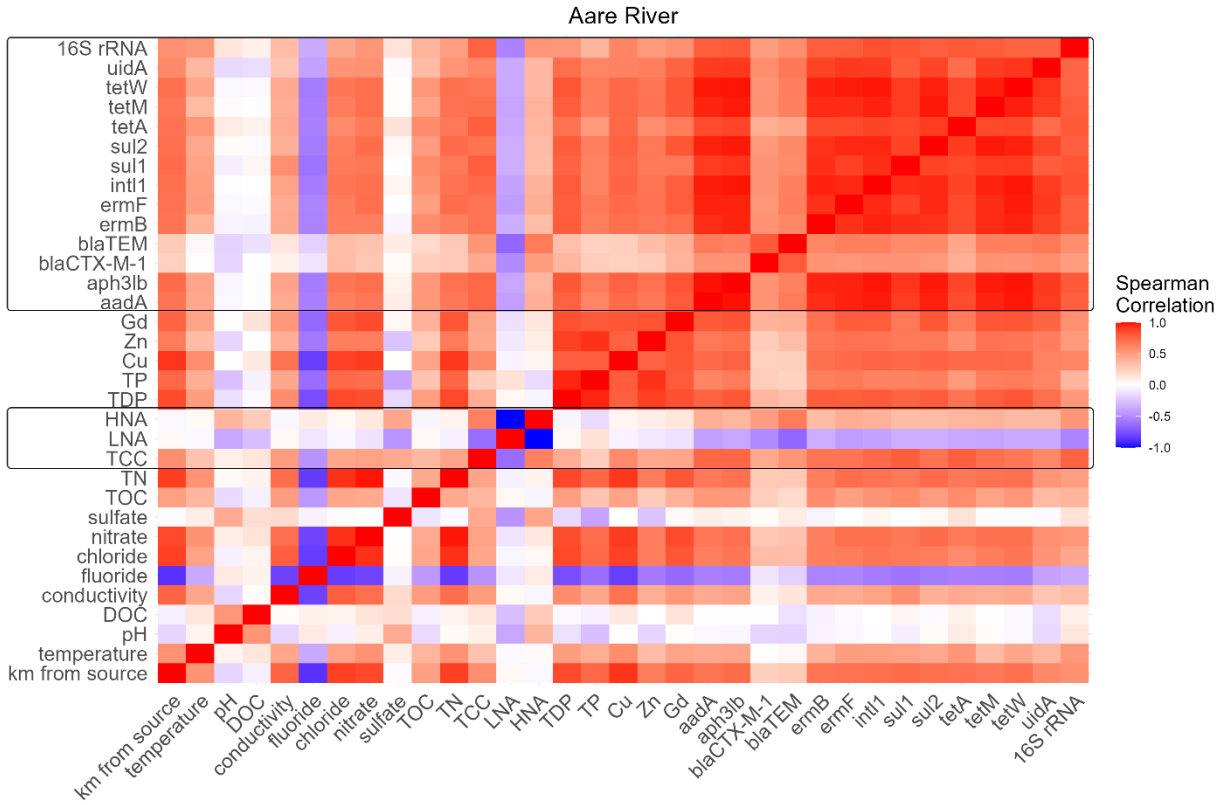

Figure 6: Heatmap of Spearman correlation matrix including quantified genes, physicochemical parameters, and biological indicators across all Aare River samples. Red: indicates strong positive correlation (ρ = 1), white: indicates no correlation (ρ = 0), blue: strong negative correlation, as one variable increases, the other decreases (ρ= -1). Black boxes include biological parameters, including FCM-derived cell counts as well as ARGs and GMs.

Correlation analysis of WWTP effluent samples revealed very strong correlations among most ARGs, including $bla_{CTX\text{-}M\text{-}1}$ and bla_{TEM}, while *tetA* consistently exhibited weak correlations (**Fig. S11**). ARGs correlated mostly positively with nutrients, metals, and bacterial abundance measures, but less closely (mostly $\rho < 0.5$) compared to river water samples. Distance was not a strong or consistent predictor for ARGs or other parameters in the WWTP effluent dataset.

4. Discussion

4.1 WWTPs are key contributors to the ARG content of the Aare river

426 Overall, observations on the River Aare were consistent with urban sources and WWTP being the
427 key contributors to ARG accumulation. For all WWTP sites studied, effluent was shown to be a
428 source of ARG relative to the receiving river water (**Fig. 5a, b**), which sufficiently explains the
429 downstream ARG increase observed near major urban centres (**Fig. S10**). This remains the case even
430 in the lower reaches of the Aare, e.g. at Aarau, where upstream contamination has accumulated
431 considerably. Accumulation of ARG also clearly exceeded the total bacteria (2.5 median DS/US
432 enrichment of *16S*) showing that ARG contamination is a specific effect distinct from bacterial cell
433 inputs.

434 Along the river continuum, two main hotspots of locally increasing ARG content at Bern and
435 Interlaken highlighted how source and sink processes can drastically affect downstream dynamics. In
436 both cases, sharp peaks in ARG absolute and relative abundance downstream of the WWTP were
437 short-lived, as the Aare entered a lake just after each city (**Fig. 4b, d, Fig. S6b, d**). The most
438 pronounced effect was observed in Bern, which was also the largest WWTP sampled. On an average,
439 effluent showed a 3.1 log higher ARG content compared to upstream water, resulting in the highest
440 downstream increase (1.6 log). WWTP Interlaken, despite operating at only one-fifth the capacity of
441 Bern, showed an even higher mean effluent ARG content relative to upstream water (3.2 log). While
442 partly explained by the comparatively pristine upstream water, the fact that Interlaken is a hotspot for
443 international tourism may have contributed to the much higher absolute abundances of ARG in
444 Interlaken compared to e.g. Thun (**Fig. 4d, 5b**). According to the local tourist association, more than
445 3.5 million overnight stays per year add substantially to the local population
446 (https://www.interlaken.ch/info-service/ueber-interlaken-tourismus/berichte-
447 statistiken/jahresberichte), with WW from visitors, residents, and the regional hospital all processed
448 by the WWTP.

449 Our results support earlier observations on the importance of WWTP discharge for ARG levels in
450 smaller Swiss rivers with proportionally high wastewater impact[24], and demonstrate this also for a
451 major river system along its full length.

452 **4.2 ARG as a component of anthropogenic impact – common sources and selection**

453 Other markers of human activity such as P and Cu (with sources in agriculture and urban wastewater)
454 increased in parallel with the AMR markers (**Fig. 2, 4**). The increase in Gd (MRI contrast agent)
455 provided an indication of healthcare activity impacts on the river, and its strong correlation with
456 ARGs indicates an additional contribution of large hospitals to the ARG input from major urban
457 centres (**Fig. 2, 6**). The overall strong correlations of ARG concentrations in river water with other
458 indicators of anthropogenic impact (**Fig. 6**) highlight ARGs as additional markers of anthropogenic
459 contamination, reflecting the cumulative influence of sustained inputs from human activity along the
460 river continuum.

461 While common sources of ARGs, metals, and nutrients primarily from wastewater discharge may
462 largely explain the observed correlations, more specific interactions such as selective effects of
463 chemical wastewater contamination should be considered[56–58]. Downstream of WWTPs, elevated
464 concentrations TDP closely mirrored ARG abundance. We observed a close correlation between
465 abundant ARG and dissolved phosphorus concentrations (TDP, $\rho > 0.7$, median 0.79), contrasting
466 with a weaker relationship of TDP with general bacterial abundance (*16S:* $\rho = 0.53$, TCC: $\rho = 0.43$).
467 A weaker relationship was observed between ARG and TN ($\rho > 0.65$, median 0.70) or TP ($\rho > 0.5$,
468 median 0.64). While P has previously been used as a proxy for bacterial growth[59], it is not considered
469 a selective agent for AMR. However, TDP increase was consistent with the observed enrichment of
470 eutrophic phyla (*Proteobacteria*, *Bacteriodota*, *Firmicutes*, *Campylobacterota*[60]), which include

471 clinically relevant genera at sites with high ARG prevalence. Such eutrophic phyla may more
472 frequently be carriers of ARGs compared to oligotrophic phyla such as *Actinobacteriota*,
473 *Planctomycetota*, and *Chloroflexi*[60] which in turn declined under high P loads. The strong co-
474 occurrence of ARGs and P likely reflects shared anthropogenic sources, such as wastewater and
475 additional diffuse agricultural inputs, and nutrient-induced alterations of the microbial community,
476 rather than a direct selective effect. Along the river (rkm 30 – 195), TP and ARG levels in
477 agriculturally impacted areas show neither a WWTP-independent increase nor a decline, suggesting
478 persistence of AMR markers or background inputs from diffuse sources (**Fig. 2a**).

479 Metals such as Cu and Zn may act as potential agents of selective pressure[61] which could explain
480 observed correlations with ARG (**Fig. 6**, **Fig. S9**). However, the measured Cu and Zn concentrations
481 in both effluents and river water (**Fig. 2b**, **Fig. S3, Table S1**) remained below experimentally
482 established thresholds required for co-selection of ARGs[62]. Nonetheless, based on reports of higher
483 levels of Cu and other metals in influent and primary clarification, selection in the upstream
484 wastewater stream cannot be excluded[63,64]. In effluents, despite low concentrations (< 10 µg/L), Cu
485 and Zn correlated positively with ARGs (ρ ~0.7 and $\rho \geq 0.6$, respectively), with the strongest
486 associations observed for *sul2* (Cu: $\rho > 0.75$), *aph(3')-lb* and *ermF* (Zn: both $\rho = 0.71$). Correlations
487 with *E. coli* marker *uidA* and bacterial marker *16S* were ~0.1 lower, indicating stronger linkage of Cu
488 to ARG-carrying subpopulations than to the overall microbial community. These findings align with
489 Miao et al.,[59] who also reported strong positive associations between heavy metals (Cu, Cr, Mn) and
490 ARG prevalence, as have several similar studies[61,65,66].

491 **4.3 ARG contamination of the Aare compared to other European rivers**

492 Can we expect a continuous accumulation of AMR along the course of major rivers? Our analysis of
493 ARG abundance in Aare River showed their absence near the source, a consistent increase towards
494 the middle and lower reaches, with pronounced regional hotspots. In contrast, while Danube
495 headwaters were likewise less impacted, no correlation between ARGs and distance (rkm) was
496 observed[36]. The Rhine likewise did not exhibit a general increase with distance; instead, regionally
497 restricted impacts were observed, particularly in the Hochrhein-Oberrhein section, attributed to the
498 river's size and buffering capacity against localized anthropogenic inputs[33]. These patterns indicate
499 that AMR contamination does not accumulate uniformly along rivers. Instead, source and sink
500 dynamics can counterbalance each other, especially in larger river systems.

501 By comparing selected marker genes that were also measured in the Rhine and Danube studies, the
502 AMR contamination in the three river systems can be compared. Even at the hotspot identified
503 downstream of Bern (rkm 124), ARG relative abundance in the Aare (*intI1*: 1.7×10^{-2}, *sul1*: 3×10^{-3}
504 copies/16S) remains below the highest values reported in the Rhine (*intI1*: 6.9×10^{0}, *sul1*: 1.07×10^{-2}
505 copies/16S)[33]. Although different β-lactamase genes were assessed in the Rhine, the relative
506 abundance at the Aare hotspot (bla_{TEM}: 5.7×10^{-5}) was comparable to bla_{SHV} levels reported in the
507 Rhine (6×10^{-5} , [33]). In addition, β-lactamases in the Rhine occurred sporadically and were closely
508 associated with WW inputs[33], aligning with our observations for $bla_{CTX\text{-}M\text{-}1}$.

509 Comparing absolute abundances, *intI1* (4.22 – 6.69 $\log_{10}$ copies/100 mL) and *sul1* (3.55 – 6.5 $\log_{10}$
510 copies/100 mL) were consistently detected at high levels across all Danube samples[32]. With the
511 exception of the more pristine Aare headwaters, where these genes were below detection, we
512 observed a comparable range (*intI1*: 3.67 – 6.03 $\log_{10}$ copies/100mL; sul1: 2.89 – 5.28 $\log_{10}$
513 copies/100mL) in the Aare. This comparison suggests that AMR contamination of the mid and lower

514 reaches of the Aare is similar or slightly lower compared to larger European rivers, underscoring the
515 substantial anthropogenic influence on the Aare.

516 In addition, load calculations showed that the Aare river acts as a major conveyor of accumulating
517 resistance genes, with only lake passages interrupting (**Fig. S7**). This further emphasizes the role of
518 the Aare in ARG dissemination within and beyond Switzerland's borders, as 8.1 x 10^9 to 5.8 x 10^{11}
519 copies/sec of the measured ARG are discharged into the Rhine river, which enters Germany roughly
520 50 km downstream of the confluence.

521 **4.4 ARG Dynamics in a complex watershed**

522 Tributaries exerted a moderate but notable effect on the ARG content of the Aare river. ARG content
523 of Aare tributaries largely reflect the size of their catchments and associated human populations. The
524 Emme, despite elevated ARG levels, contributed only modestly due to its relatively low discharge;
525 the subsequent rise in ARGs downstream could be more likely attributed to effluent from WWTP
526 Solothurn. In contrast, the Reuss and Limmat, both with large catchments and daily discharges >100
527 m^3/sec (each almost 50% of the Aare discharge before their confluence) exerted a much stronger
528 hydrological and microbial influence. Their combined effect was dilution of ARG levels (**Fig. 4**),
529 while maintaining a high total ARG load (**Fig. S7**), as Aare's discharge nearly doubled downstream
530 of these confluences (from 270 to 515 m^3/sec, **Fig. S2**). These observations underscore the critical
531 role of absolute discharge volume on ARG distribution and dissemination.

532 Lakes, in contrast, behaved consistently as sinks, producing a pronounced "reset effect" on riverine
533 ARG abundance, documented here for the first time. After passage through lakes, ARG
534 concentrations decreased by up to 1.5 log units, with certain genes becoming undetectable in the lake

535 outflow. These reductions appear further enhanced by high water residence time, with near-complete
536 removal in Thunersee (648 days[67]) compared to partial reduction in Bielersee (58 days[67]), despite
537 similar upstream ARG concentrations (**Fig. 4**). Notably, Wohlensee, a reservoir with a retention time
538 of only 2.1 days[68], substantially attenuated the high ARG concentrations entering from downstream
539 of Bern. Earlier work by Czekalski et al. linked WWTP capacity in the catchment with ARG content
540 in Swiss lakes[69], showing that Swiss lakes are not insulated from upstream ARG inputs. The present
541 study adds that lakes are simultaneously major ARG sinks. In large lakes with long water residence
542 time, this likely reflects gradual replacement of the river microbiome by lake-adapted communities
543 over time scales of months to years. The rapid response observed in Wohlensee suggests additional
544 sink mechanisms acting on shorter timescale (days) such as sedimentation (of particle-bound cells or
545 cell aggregates), predation, or UV-mediated decay of resistant communities under reduced flow
546 conditions.

547 **Conclusion**

548 Integration of genetic AMR markers with microbial and chemical parameters along the full course of
549 the Aare River enabled us to capture spatial dynamics, identify hotspots and sinks, and link resistance
550 patterns to anthropogenic inputs. Our findings demonstrate that ARG levels are shaped by WW
551 discharges and cumulative anthropogenic pressures along the entire river, positioning the Aare as a
552 critical interface for potential AMR transmission. Our results further highlight the dynamic impact of
553 lakes and tributaries on the main river. While tributaries can influence ARG levels through both inputs
554 and dilution, lakes function as effective sinks that substantially reduce ARG concentrations. The
555 behaviour observed in Wohlensee highlights how in-lake ARG dynamics remain poorly understood
556 and require further investigation.

557 We also demonstrate that reporting absolute abundance (concentration), relative abundance, and total
558 load (fluxes) of ARGs are each important parameters to assess the AMR situation of a river system
559 and should be reported in such studies to improve comparability. This comprehensive dataset
560 establishes a valuable baseline not only for Switzerland but also for comparable river systems,
561 emphasizing the need for targeted management interventions. In the context of ongoing and planned
562 nationwide upgrades in WW treatment for organic micropollutant removal by 2040, the effectiveness
563 of these measures should be evaluated also with respect to ARG reduction in receiving waters.
564 Moving forward, studies that explicitly address transmission potential and risk assessment are
565 essential. Collectively, these findings highlight that rivers function not only as passive recipients but
566 also as active conduits of AMR, with implications that extend beyond national borders.

567

Acknowledgments

We thank the staff at the WWTPs in Interlaken, Thun, Bern, Biel, Lyss, Centravo AG at Lyss, Solothurn, Aarau, Oensingen and Baden for allowing and supporting effluent sampling at their facilities. We thank Antonia Zuber and Urs Lergster for the technical assistance with DNA extractions and qPCR (both Eawag, Switzerland). We thank Patrick Kathriner for performing TN, and TOC measurements, Marcel Walter for performing ICP-MS measurements, at the Aquatic Geochemistry lab at Eawag in Kastanienbaum and AuA-Lab (Analytik- und Ausbildungslabor) at Eawag Dübendorf for measuring anions by ion chromatography. We thank Dr. Martin Schmid and James Runnalls (both Eawag, Switzerland) for assisting with access to additional metadata from MetoSchweiz/Idaweb and Federal Office for the Environment (Bundesamt für Umwelt; BAFU) hydrological data, respectively. We thank Prof. Damien Bouffard (Eawag, Kastanienbaum, Switzerland) and Dr. Massimiliano Zappa (WSL, Switzerland) for valuable feedback and input on our discharge model for the Aare river. We thank Andreas Scheidegger (Statistics, Data Science & Modeling, Eawag, Dübendorf, Switzerland) for consultations regarding statistical analysis and Tara Behnsen (Surface Waters- Research and Management, Eawag, Kastanienbaum, Switzerland) and Rosi Siber (Statistics, Data Science & Modeling, Eawag, Dübendorf, Switzerland) for consultation regarding QGIS visualization and analysis.

Author Contributions

Conceptualization: DLW & HB (general study and all components except trace metals); DJJ (trace metal component). **Funding acquisition**: HB. **Investigation**: DLW; JA & NJA (trace metal component). **Methodology**: KB, SR, DLW, HB; DJJ (trace metal component). **Data curation**: DLW, HB. **Formal analysis**: DLW; JA & DJJ (trace metal component). **Visualization**: DLW. **Software**: DLW, SR, HB. **Writing – original draft**: DLW. **Writing – review & editing**: all authors. **Supervision**: HB, KB; DJJ (trace metal component). **Project administration**: DLW, HB. **Resources**: HB; DJJ (trace metal component).

Data Availability

Raw sequence reads of bacterial 16S rRNA gene amplicons are available from the NCBI Sequence Read Archive under BioProject PRJNA1375744. All other processed data required to reproduce the above findings are available in the manuscript and the supplementary tables.

Competing interests

The authors have no competing interests to declare.

602

603 **References**

604 1. Murray, C. J. Global burden of bacterial antimicrobial resistance in 2019: a systematic analysis. *Lancet*
605 *(London, England)* **399,** 629–655; 10.1016/S0140-6736(21)02724-0 (2022).

606 2. O'Neill, J. Antimicrobial resistance: tackling a crisis for the health and wealth of nations. *Rev.*
607 *Antimicrob. Resist.* (2014).

608 3. O'Neill, J. *Tackling drug-resistant infections globally: final report and recommendations* (2016).

609 4. Niegowska, M., Sanseverino, I., Navarro, A. & Lettieri, T. Knowledge gaps in the assessment of
610 antimicrobial resistance in surface waters. *FEMS microbiology ecology* **97**; 10.1093/femsec/fiab140
611 (2021).

612 5. Raaijmakers, J. M. & Mazzola, M. Diversity and natural functions of antibiotics produced by beneficial
613 and plant pathogenic bacteria. *Annual review of phytopathology* **50,** 403–424; 10.1146/annurev-phyto-
614 081211-172908 (2012).

615 6. Ezebialu, C. U. *et al.* Screening and Characterization of Antibiotic Producing Organisms from Waste
616 Dump Soil Sample. *AiM* **10,** 422–433; 10.4236/aim.2020.109031 (2020).

617 7. Hwengwere, K. *et al.* Antimicrobial resistance in Antarctica: is it still a pristine environment?
618 *Microbiome* **10,** 71; 10.1186/s40168-022-01250-x (2022).

619 8. Andersson, D. I. & Hughes, D. Evolution of antibiotic resistance at non-lethal drug concentrations.
620 *Drug resistance updates : reviews and commentaries in antimicrobial and anticancer chemotherapy* **15,**
621 162–172; 10.1016/j.drup.2012.03.005 (2012).

622 9. Martin, M. J., Thottathil, S. E. & Newman, T. B. Antibiotics Overuse in Animal Agriculture: A Call to
623 Action for Health Care Providers. *American journal of public health* **105,** 2409–2410;
624 10.2105/AJPH.2015.302870 (2015).

625 10. Federal Office of Public Health, Swiss Confederation & Federal Food Safety and Veterinary Office.
626 Swiss Antibiotic Resistance Report 2024 (2024).

11. Janssens, I., Tanghe, T. & Verstraete, W. Micropollutants: a bottleneck in sustainable wastewater treatment. *Water Science and Technology* **35,** 13–26; 10.2166/wst.1997.0349 (1997).

12. Pruden, A., Pei, R., Storteboom, H. & Carlson, K. H. Antibiotic resistance genes as emerging contaminants: studies in northern Colorado. *Environmental science & technology* **40,** 7445–7450; 10.1021/es060413l (2006).

13. Sarmah, A. K., Meyer, M. T. & Boxall, A. B. A. A global perspective on the use, sales, exposure pathways, occurrence, fate and effects of veterinary antibiotics (VAs) in the environment. *Chemosphere* **65,** 725–759; 10.1016/j.chemosphere.2006.03.026 (2006).

14. Savin, M. *et al.* Antibiotic-resistant bacteria and antimicrobial residues in wastewater and process water from German pig slaughterhouses and their receiving municipal wastewater treatment plants. *The Science of the total environment* **727,** 138788; 10.1016/j.scitotenv.2020.138788 (2020).

15. Bürgmann, H. *et al.* Water and sanitation: an essential battlefront in the war on antimicrobial resistance. *FEMS microbiology ecology* **94**; 10.1093/femsec/fiy101 (2018).

16. Rizzo, L. *et al.* Urban wastewater treatment plants as hotspots for antibiotic resistant bacteria and genes spread into the environment: a review. *The Science of the total environment* **447,** 345–360; 10.1016/j.scitotenv.2013.01.032 (2013).

17. Marano, R. B. M. *et al.* A global multinational survey of cefotaxime-resistant coliforms in urban wastewater treatment plants. *Environment international* **144,** 106035; 10.1016/j.envint.2020.106035 (2020).

18. Ju, F. *et al.* Wastewater treatment plant resistomes are shaped by bacterial composition, genetic exchange, and upregulated expression in the effluent microbiomes. *ISME J* **13,** 346–360; 10.1038/s41396-018-0277-8 (2019).

19. Read, D. S. *et al.* Dissemination and persistence of antimicrobial resistance (AMR) along the wastewater-river continuum. *Water research* **264,** 122204; 10.1016/j.watres.2024.122204 (2024).

20. Jäger, T. *et al.* Reduction of Antibiotic Resistant Bacteria During Conventional and Advanced Wastewater Treatment, and the Disseminated Loads Released to the Environment. *Frontiers in microbiology* **9,** 2599; 10.3389/fmicb.2018.02599 (2018).

21. S. Djordjevic & Branwen Morgan. A One Health genomic approach to antimicrobial resistance is essential for generating relevant data for a holistic assessment of the biggest threat to public health. *Microbiology Australia* (2019).

22. Lee, J., Ju, F., Beck, K. & Bürgmann, H. Differential effects of wastewater treatment plant effluents on the antibiotic resistomes of diverse river habitats. *ISME J* **17,** 1993–2002; 10.1038/s41396-023-01506-w (2023).

23. Pruden, A., Arabi, M. & Storteboom, H. N. Correlation between upstream human activities and riverine antibiotic resistance genes. *Environmental science & technology* **46,** 11541–11549; 10.1021/es302657r (2012).

24. Lee, J. *et al.* Unraveling the riverine antibiotic resistome: The downstream fate of anthropogenic inputs. *Water research* **197,** 117050; 10.1016/j.watres.2021.117050 (2021).

25. Bundesamt für Umwelt BAFU. Abwasserfinanzierung / Abwasserfonds. Available at https://www.bafu.admin.ch/bafu/de/home/themen/wasser/fachinformationen/massnahmen-zum-schutz-der-gewaesser/abwasserreinigung/abwasserfinanzierung_abwasserfonds.html (2023).

26. Joss, A. *et al.* Biological degradation of pharmaceuticals in municipal wastewater treatment: proposing a classification scheme. *Water Research* **40,** 1686–1696; 10.1016/j.watres.2006.02.014 (2006).

27. Knapp, C. W., Dolfing, J., Ehlert, P. A. I. & Graham, D. W. Evidence of increasing antibiotic resistance gene abundances in archived soils since 1940. *Environmental science & technology* **44,** 580–587; 10.1021/es901221x (2010).

28. Berendonk, T. U. *et al.* Tackling antibiotic resistance: the environmental framework. *Nat Rev Microbiol* **13,** 310–317; 10.1038/nrmicro3439 (2015).

29. Leonard, A. F. C., Zhang, L., Balfour, A. J., Garside, R. & Gaze, W. H. Human recreational exposure to antibiotic resistant bacteria in coastal bathing waters. *Environment international* **82,** 92–100; 10.1016/j.envint.2015.02.013 (2015).

30. Xie, J. *et al.* Bacteria and Antibiotic Resistance Genes (ARGs) in PM2.5 from China: Implications for Human Exposure. *Environmental science & technology* **53,** 963–972; 10.1021/acs.est.8b04630 (2019).

31. Weingartner, R. & Viviroli, D. Die Alpen – das Wasserschloss Europas, 2002.

681 32. Schachner-Groehs, I. *et al.* Linking antibiotic resistance gene patterns with advanced faecal pollution
682 assessment and environmental key parameters along 2300 km of the Danube River. *Water research*
683 **252,** 121244; 10.1016/j.watres.2024.121244 (2024).

684 33. Paulus, G. K., Hornstra, L. M. & Medema, G. International tempo-spatial study of antibiotic resistance
685 genes across the Rhine river using newly developed multiplex qPCR assays. *The Science of the total*
686 *environment* **706,** 135733; 10.1016/j.scitotenv.2019.135733 (2020).

687 34. Peng, F. *et al.* Urbanization drives riverine bacterial antibiotic resistome more than taxonomic
688 community at watershed scale. *Environment international* **137,** 105524; 10.1016/j.envint.2020.105524
689 (2020).

690 35. Jiang, C., Zhao, Z., Zhu, D., Pan, X. & Yang, Y. Rare resistome rather than core resistome exhibited
691 higher diversity and risk along the Yangtze River. *Water research* **249,** 120911;
692 10.1016/j.watres.2023.120911 (2024).

693 36. Gao, F.-Z. *et al.* Integrating global microbiome data into antibiotic resistance assessment in large rivers.
694 *Water research* **250,** 121030; 10.1016/j.watres.2023.121030 (2024).

695 37. Lee, K. *et al.* Mobile resistome of human gut and pathogen drives anthropogenic bloom of antibiotic
696 resistance. *Microbiome* **8,** 2; 10.1186/s40168-019-0774-7 (2020).

697 38. Neher, T. P., Ma, L., Moorman, T. B., Howe, A. C. & Soupir, M. L. Catchment-scale export of
698 antibiotic resistance genes and bacteria from an agricultural watershed in central Iowa. *PloS one* **15,**
699 e0227136; 10.1371/journal.pone.0227136 (2020).

700 39. Bundesamt für Umwelt BAFU. Hydrologische Daten und Vorhersagen. Available at
701 https://www.hydrodaten.admin.ch/de/aktuelle-lage (2025).

702 40. Nyall Dawson *et al. qgis/QGIS: 3.36.1* (Zenodo, 2025).

703 41. Federal Office of Public Health, Swiss Confederation. SLMB. Determining the total cell count and
704 ratios of high and low nucleic acid content cells in freshwater using flow cytometry. Available at
705 https://www.admin.ch/gov/en/start/documentation/media-releases.msg-id-47549.html (2012).

706 42. Proctor, C. R. *et al.* Phylogenetic clustering of small low nucleic acid-content bacteria across diverse
707 freshwater ecosystems. *The ISME journal* **12,** 1344–1359; 10.1038/s41396-018-0070-8 (2018).

43. Chern, E. C., Siefring, S., Paar, J., Doolittle, M. & Haugland, R. A. Comparison of quantitative PCR assays for Escherichia coli targeting ribosomal RNA and single copy genes. *Letters in applied microbiology* **52,** 298–306; 10.1111/j.1472-765X.2010.03001.x (2011).

44. Chern, E. C., Brenner, K. P., Wymer, L. & Haugland, R. A. Comparison of Fecal Indicator Bacteria Densities in Marine Recreational Waters by QPCR. *Water Expo. Health* **1,** 203–214; 10.1007/s12403-009-0019-2 (2009).

45. Czekalski, N., Berthold, T., Caucci, S., Egli, A. & Bürgmann, H. Increased levels of multiresistant bacteria and resistance genes after wastewater treatment and their dissemination into lake geneva, Switzerland. *Frontiers in microbiology* **3,** 106; 10.3389/fmicb.2012.00106 (2012).

46. Rathinavelu, S., Beck, K., Wälchli, D. L. & Bürgmann, H. Optimization and validation of a consolidated Set of TaqMan qPCR assays for the surveillance of clinically relevant antibiotic resistance genes in environmental matrices. *MethodsX* **15,** 103600; 10.1016/j.mex.2025.103600 (2025).

47. Curry, K. D. *et al.* Emu: species-level microbial community profiling of full-length 16S rRNA Oxford Nanopore sequencing data. *Nat Methods* **19,** 845–853; 10.1038/s41592-022-01520-4 (2022).

48. Janssen, D. J. *et al.* Biogeochemical cycling of trace elements and nutrients in ferruginous waters: Constraints from a deep oligotrophic ancient lake. *Limnology & Oceanography* **69,** 2775–2790; 10.1002/lno.12687 (2024).

49. Federal Office for the Environmnet, Swiss Confederation. Hydrological data and forecasts: Discharge and water level. Available at https://www.hydrodaten.admin.ch/en/seen-und-fluesse/messstationen-zustand (2025).

50. R Core Team. *R: A Language and Environment for Statistical Computing* (R Foundation for Statistical Computing, Vienna, Austria, 2024).

51. Posit team. *RStudio: Integrated Development Environment for R.* (Posit Software, PBC, Boston, Ma, 2024).

52. Oksanen J, Simpson G, Blanchet F, Kindt R, Legendre P, Minchin P, O'Hara R, Solymos P, Stevens M. *vegan: Community Ecology Package* (2022).

53. Callender, E. & Rice, K. C. The Urban Environmental Gradient: Anthropogenic Influences on the Spatial and Temporal Distributions of Lead and Zinc in Sediments. *Environ. Sci. Technol.* **34,** 232–238; 10.1021/es990380s (2000).

54. Comber, S. *et al.* Sources of copper into the European aquatic environment. *Integrated environmental assessment and management* **19,** 1031–1047; 10.1002/ieam.4700 (2023).

55. Bau, M. & Dulski, P. Anthropogenic origin of positive gadolinium anomalies in river waters. *Earth and Planetary Science Letters* **143,** 245–255; 10.1016/0012-821X(96)00127-6 (1996).

56. Di Cesare, A. *et al.* Co-occurrence of integrase 1, antibiotic and heavy metal resistance genes in municipal wastewater treatment plants. *Water research* **94,** 208–214; 10.1016/j.watres.2016.02.049 (2016).

57. Guo, X. *et al.* Behavior of antibiotic resistance genes under extremely high-level antibiotic selection pressures in pharmaceutical wastewater treatment plants. *The Science of the total environment* **612,** 119–128; 10.1016/j.scitotenv.2017.08.229 (2018).

58. Raza, S., Shin, H., Hur, H.-G. & Unno, T. Higher abundance of core antimicrobial resistant genes in effluent from wastewater treatment plants. *Water research* **208,** 117882; 10.1016/j.watres.2021.117882 (2022).

59. Miao, J. *et al.* Assessing the nonlinear association of environmental factors with antibiotic resistance genes (ARGs) in the Yangtze River Mouth, China. *Sci Rep* **13,** 20367; 10.1038/s41598-023-45973-9 (2023).

60. Xie, G., Zhang, Y., Gong, Y., Luo, W. & Tang, X. Extreme trophic tales: deciphering bacterial diversity and potential functions in oligotrophic and hypereutrophic lakes. *BMC Microbiology* **24,** 348; 10.1186/s12866-024-03488-x (2024).

61. Seiler, C. & Berendonk, T. U. Heavy metal driven co-selection of antibiotic resistance in soil and water bodies impacted by agriculture and aquaculture. *Front. Microbiol.* **3,** 399; 10.3389/fmicb.2012.00399 (2012).

62. Kang, W., Zhang, Y.-J., Shi, X., He, J.-Z. & Hu, H.-W. Short-term copper exposure as a selection pressure for antibiotic resistance and metal resistance in an agricultural soil. *Environmental science and pollution research international* **25,** 29314–29324; 10.1007/s11356-018-2978-y (2018).

63. Agoro, M. A., Adeniji, A. O., Adefisoye, M. A. & Okoh, O. O. Heavy Metals in Wastewater and Sewage Sludge from Selected Municipal Treatment Plants in Eastern Cape Province, South Africa. *Water* **12,** 2746; 10.3390/w12102746 (2020).

64. Chen, A. *et al.* Proliferation of Resistance Genes in Wastewater Pipe Under Tetracycline and Cu Stress. *Water environment research : a research publication of the Water Environment Federation* **97,** e70155; 10.1002/wer.70155 (2025).

65. Dickinson, A. W. *et al.* Heavy metal pollution and co-selection for antibiotic resistance: A microbial palaeontology approach. *Environment international* **132,** 105117; 10.1016/j.envint.2019.105117 (2019).

66. Di Cesare, A., Eckert, E. & Corno, G. Co-selection of antibiotic and heavy metal resistance in freshwater bacteria. *J Limnol* **75**; 10.4081/jlimnol.2016.1198 (2016).

67. Runnalls, J. Alplakes v2.0. Available at https://www.alplakes.eawag.ch/ (2025).

68. Albrecht, A., Reiser, R., Lück, A., Stoll, J.-M. A. & Giger, W. Radiocesium Dating of Sediments from Lakes and Reservoirs of Different Hydrological Regimes. *Environ. Sci. Technol.* **32,** 1882–1887; 10.1021/es970946h (1998).

69. Czekalski, N., Sigdel, R., Birtel, J., Matthews, B. & Bürgmann, H. Does human activity impact the natural antibiotic resistance background? Abundance of antibiotic resistance genes in 21 Swiss lakes. *Environment international* **81,** 45–55; 10.1016/j.envint.2015.04.005 (2015).

Supplementary Material for:

Ripples of Resistance: Unveiling Antimicrobial Resistance Dynamics Along Switzerland's Aare River

Denise Lea Wälchli[1,2], Sasikaladevi Rathinavelu[1], Jane Ackeret[1,3], Norberto Jr Aquino[1,4], Karin Beck[1], David Janssen[1], Helmut Bürgmann[1,*]

[1]Eawag, Swiss Federal Institute of Aquatic Science and Technology, Kastanienbaum, Switzerland

[2] Department of Plant and Microbial Biology, University of Zurich, Zurich, Switzerland

[3] Department of Environmental Systems Science, ETH Zurich, Zurich, Switzerland

[4] Department of Civil, Environmental and Natural Resources Engineering, Luleå University of Technology, Luleå, Sweden

[*]Corresponding author email contact: helmut.buergmann@eawag.ch

S1. Supplementary Material and Methods

S1.1 Description of the study area

The Aare is Switzerland's longest river, passes through the cantons Bern, Solothurn, and Aargau, draining approximately 43 % of the country (catchment size: 17'709 km^2). Originating in a largely untouched alpine region (**Fig. 1a**), fed by the Unteraar and Oberaar glaciers, the Aare River flows through a mountain valley with several villages before entering Brienzersee (29.81 km^2) and shortly after Thunersee (47.74 km^2) - two alpine lakes, shaped by the alpine climate and inflows from numerous mountain creeks, but also the cities of Interlaken and Thun. Downstream, the river traverses foothill landscapes of the Swiss Alps, transitioning into a mix of agricultural land and scattered settlements, with urban centres concentrated around Bern and Biel. Between them lies Wohlensee (3.65 km^2), a slow-flowing hydropower reservoir built in a Molasse gorge, and Bielersee (39.51 km2), one of three large Jura lakes in the agriculturally productive Seeland region, fed by the Zihl canal and Jura mountain streams. From Thun to Solothurn, the river passes mainly agricultural areas, interspersed with small towns. East of Solothurn is the confluence with the Emme, a minor tributary by discharge but with a 900 km^2 catchment area, over half of which is farmland, originating in the Emmental Alps. Beyond Solothurn, agricultural land becomes less dominant as settlements become denser and more industrialized, particularly in the canton Aargau, before the Aare meets two major tributaries: The Reuss (draining central Switzerland) and the Limmat (draining the northeastern Alps), join the Aare before it discharges into the Rhine near Koblenz. At the confluence, the Aare River contributes more discharge than the upper Rhine.

S1.2 Flow Cytometry (FCM)

Measurements were performed on a NovoCyte Advanteon flow cytometer (Agilent, USA). For each measurement, 50 mL aliquots were taken from the original sample and stored at 4 °C until measurement (storing up to 3 days post sample collection). To prevent nozzle clogging, visibly turbid samples were passed through a 40 µm nylon Cell Strainer (Falcon, Thermo Fisher Scientific, USA) pre-measurement. As negative control, sterile-filtered Evian water purchased from the local store was used. The gating strategies for determination of total cell counts (TCC) and the high nucleic acid (HNA) and low nucleic acid (LNA) fractions are displayed in **S2, Fig. S1**.

S1.3 Quantitative PCR (qPCR)

qPCR assays met established quality criteria for linearity ($R^2 > 0.99$) and efficiency (90 - 110%), except for tetA ($R^2 = 0.981$) (**Tab. S7**). Slopes between -3.1 and -3.6 correspond to efficiencies between 90% and 110%, which were considered acceptable (**Tab. S7**). However, only minimal effects on measurement results are expected for the diluted samples, therefore results were normally evaluated. Negative and extraction controls were either negative or showed Cp values above the lowest standard (50 copies/reaction). Values above the LOQ were not extrapolated but set to zero to ensure consistency across genes. Outliers were excluded when standard deviations of triplicate Cp exceeded 0.5, which occurred only for values >LOQ.

Corresponding primer and fluorescence probe sequences for Taq Man assays (LightCycler 480 Probes Master; Roche, Switzerland) were adapted from internal protocols and Rathinavelu et al. (2025), except for *ermB*, $bla_{CTX\text{-}M\text{-}1}$, and *qnrA*, which were analyzed using SYBR Green assay (LightCycler 480 SYBR Green Master; Roche, Switzerland). As standards for the genes $bla_{CTX\text{-}M\text{-}1}$, *ermB*, *sul1*, *sul2*, *tetM*, *tetW*, *qnrA*, *intl1* and *16S rRNA*, plasmid harboring cloned inserts of the target genes, each carrying the respective target indicator gene, was utilized. Synthetic gBlock DNA, published by Rathinavelu et al. (2025) [1] served as standards for the genes *aadA*, *aph(3')lb*, bla_{TEM}, *ermF*, *mcr1*, *mecA*, *tetA,* and *uidA.* All sequences and cycling conditions are summarized in **Tables S3-S7**.

S1.4 16S rRNA Gene Amplicon Sequencing

Amplicons were generated using the PCR cDNA barcoding kit SQK-PCB111.24 (Oxford Nanopore Technologies, UK). Undiluted DNA extracts served as templates for amplification of 16S rRNA gene (V3-V4 region) following a modified two-step PCR protocol.

PCR-1 (25 µL) contained 12.5 µL PCR mix, 9.5 µL nuclease-free water, 1 µL of each primers 341F and 806R (10 µM), and 1 µL template DNA (2 µL if concentration <10 ng/µL). Cycling conditions were 95 °C for 30 s, followed by 30 cycles of 95 °C for 15 s, 55 °C for 15 s, 65 °C for 30 s, and a final extension at 65 °C for 6 min, yielding ~460 bp amplicons. PCR-2 (25 µL) used 5 µL of PCR-1 product, 12.5 µL PCR mix, 6.75 µL nuclease-free water, and 0.75 µL barcoded primers (cDNA barcoding kit). Cycling conditions were 95 °C for 30 s, followed by 15 cycles of 95 °C for 15 s, 62 °C for 15 s, 65 °C for 40 s, and a final extension at 65 °C for 6 min, generating ~620 bp fragments. PCR products were purified with AMPure XP magnetic beads (1 µL per 1 µL PCR reaction), washed twice with 70% ethanol, and eluted in 10 µL Tris-HCl buffer (pH 8). Purified amplicons were quantified with a NanoDrop One spectrophotometer (Thermo Fisher Scientific, USA), diluted to 10 ng/µL, and pooled (≤ 100 ng total DNA per flow cell) for sequencing.

The primer pair 341f (5'-TTT CTG TTG GTG CTG ATA TTG CCC TAC GGG NGG CWG CAG-3') and 806r (5'-ACT TGC CTG TCG CTC TAT CTT CGG ACT ACH VGG GTW TCT AAT-3') targeted the V3 and V4 regions. Core primer sequences were originally published by Klindworth et al. and subsequently adapted in-house for improved coverage of wastewater microbiomes. Five samples failing initial library QC, likely due to matrix-related inhibition, were successfully resequenced after 10-fold dilution. Prior to sequencing, barcoded DNA libraries were pooled in equimolar ratios, and sequenced to a minimum depth of 30'000 reads per sample, with most libraries yielding 40'000 to 76'000 reads in accordance with the manufacturer's quality standards. Reads with a Q value <10 were rejected. Median Q values per run varied between 13 and 15 per run.

FASTQ data was analyzed using the EMU software (version 3.4.5) in the MiniConda environment (version 3) using the SILVA database (Release 138, Ref Nr. 99). Data was imported into R (version 2024.04.2) and formatted for use with the Phyloseq package (by McMurdie et al.[2]) with a custom script and analyzed in R (see **Chapter 2.8**). Prior to analysis, non-bacterial sequences (such as mitochondria, chloroplasts, and eukaryotes) as well as unassigned reads, were removed.

S1.5 Metal, Chemical, and Nutrient Parameters

For nutrient analysis, 50 mL aliquots were collected in Falcon tubes to measure nutrients (TN, TP) and dissolved anions. Additionally, 10 mL aliquots were collected in glass vials for the analysis of TOC and acidified with 32% HCl in the field. Samples were stored at 4°C. For the measurement, using a Shimadzu (Japan) TOC-L analyzer, 100 mg/L C NPOC working standard solution, 100 mg/L N TN standard solution, and control solution NPOC/TN (QC 5 ppm) were prepared according to ISO 1484:1979 and ISO 11905-1:1998. Blank vials containing nanopure water enriched with 32% HCl were used. Samples and calibration standards for TP were prepared according to ISO 15681-1:2003 followed by measurements using flow-injection analysis Skalar San ++ complete system (Procon AG, Switzerland).

For metal trace quantification, samples were dried at 100 °C, digested with 0.25 mL sub-boiled HNO_3 at 120 °C for ≥ 6 h, re-dried, and re-dissolved in 5 mL 0.2 M HNO_3. Aliquots were transferred into acid-cleaned 15 mL polypropylene tubes for mass spectrometry analysis using an Agilent 8900 ICP-MS/MS instrument. Helium, H_2, and O_2 gases were used in a collision cell or as reaction gasses to minimize interferences Measurements were conducted in four batches (Sept. 2024 – Apr. 2025) with procedural blanks and certified reference material (SLRS-6) see Tab. S10. Calibration curves were prepared gravimetrically, and samples and standards were corrected via internal standardization using Rh. Additional details on analytical parameters and modes are presented in Janssen et al. (2024)[3]

S2. Supplementary Figures

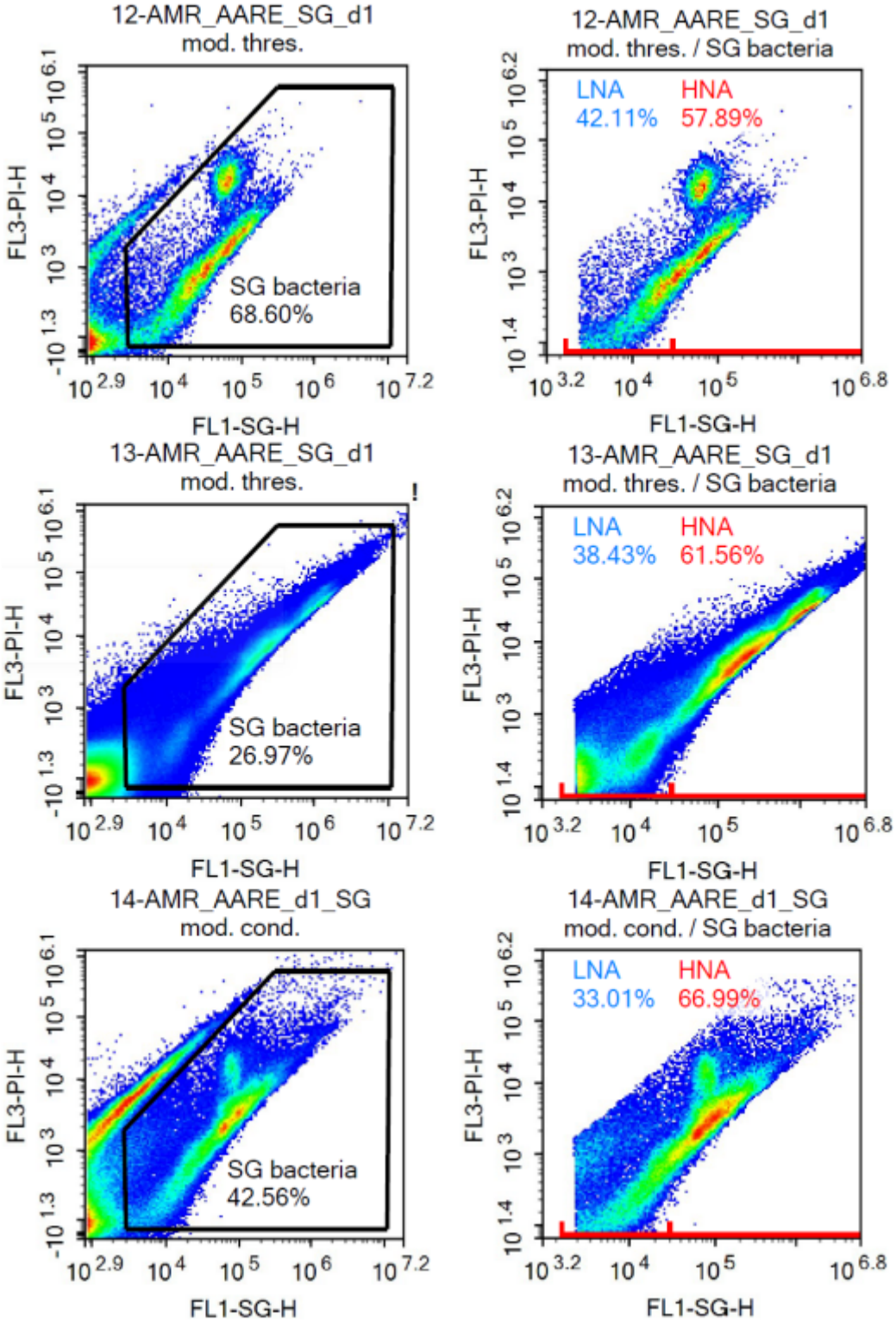

Figure S1: Example scatter plots of the fluorescence intensity of the particles determined by flow cytometry and the gate used for the total cell count determination (SG bacteria) and high and low nucleic acid content (HNA/LNA) of three samples. FL1-SG-H: Fluorescence intensity at the wavelength of the SYBRgreen-DNA complex. FL3-PI-H: Intensity of the nonspecific autofluorescence. Each point corresponds to a cell detection, with colors ranging from blue to red indicating accumulated signals. FCM-patterns of populations downstream of the discharge point (DS: #14) is considerably altered compared to the location upstream of the WWTP (US: #12). It shows similarities to the effluent of the treatment plant (EFF: #13).

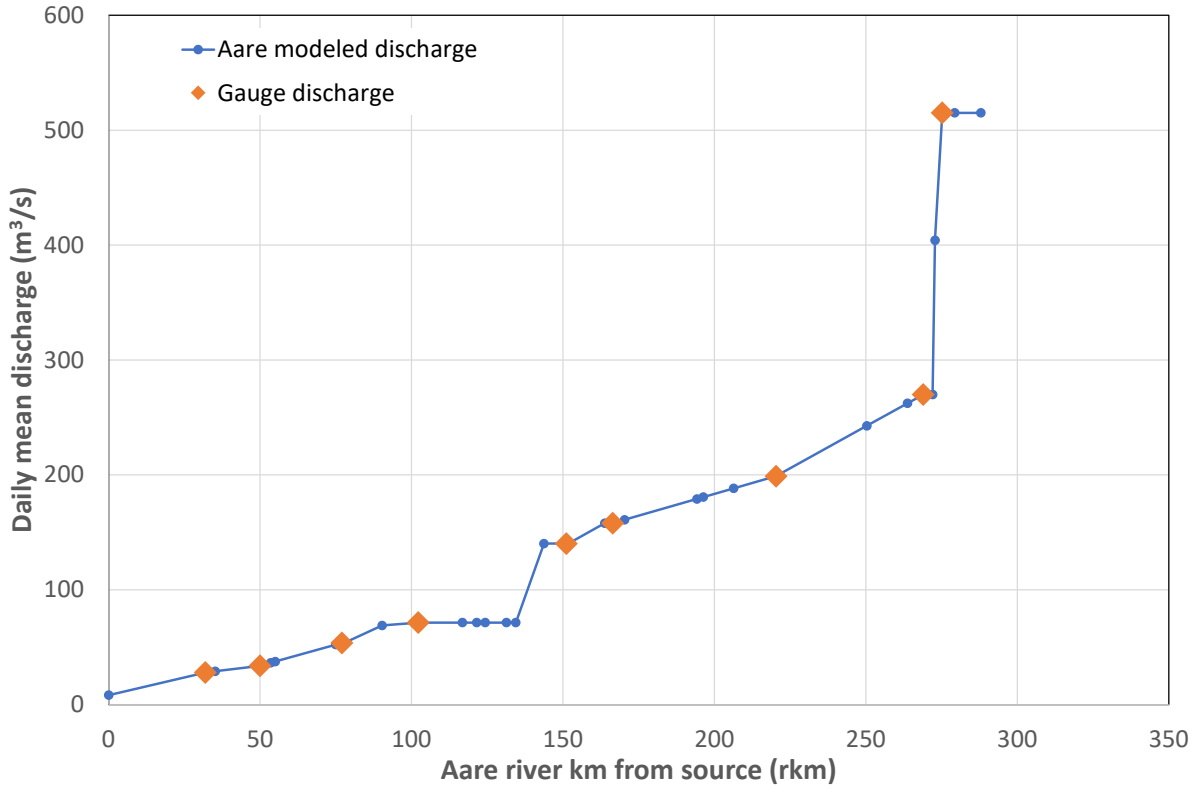

Figure S2: Modeled mean daily discharge of the Aare river at sampling points. Gauge discharge values (orange diamonds) were obtained for the day of sampling the nearby river reaches, see **Table S12**. Values for sampling locations (blue) were obtained by constructing a discharge model using interpolation and taking into account input from major tributaries, see **Table S13**.

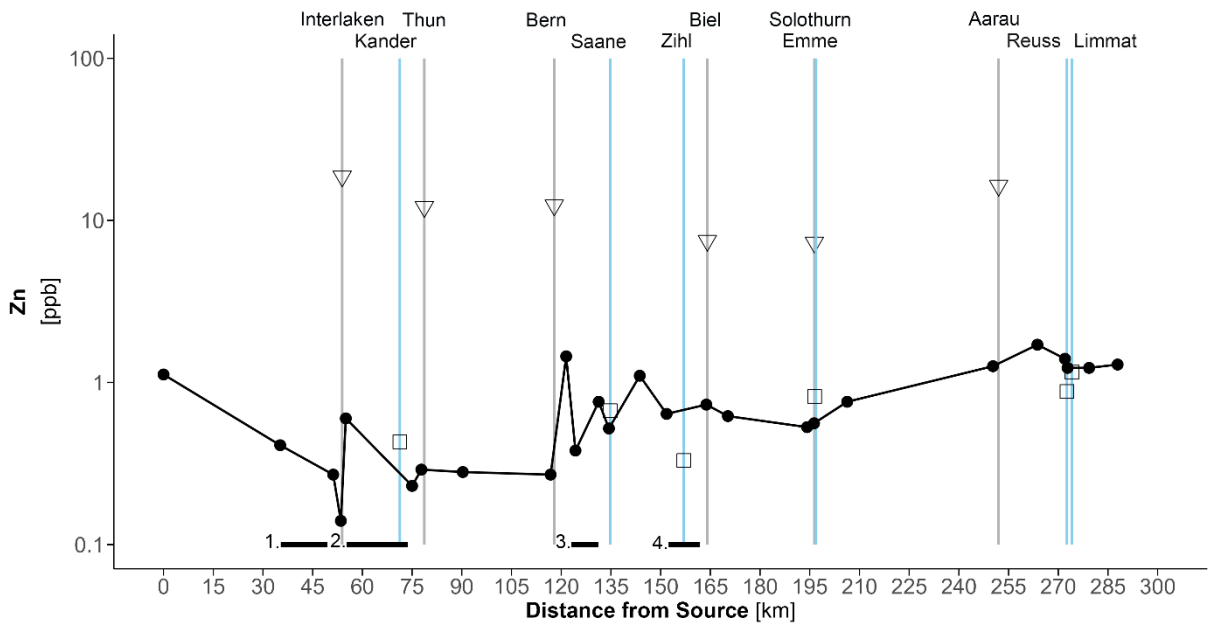

Figure S3: Zinc (Zn) concentrations along the Aare River. Continuous black lines represent Zn concentrations in river water along the river course. Triangles on grey bars indicate concentrations in WWTP effluents, and squares on blue bars show inputs from tributaries. Flow-through lakes are shown as black bars on the x-axis: 1) Brienzersee, 2) Thunersee, 3) Wohlensee, and 4) Bielersee. Major tributaries and corresponding WWTPs are labled on top.

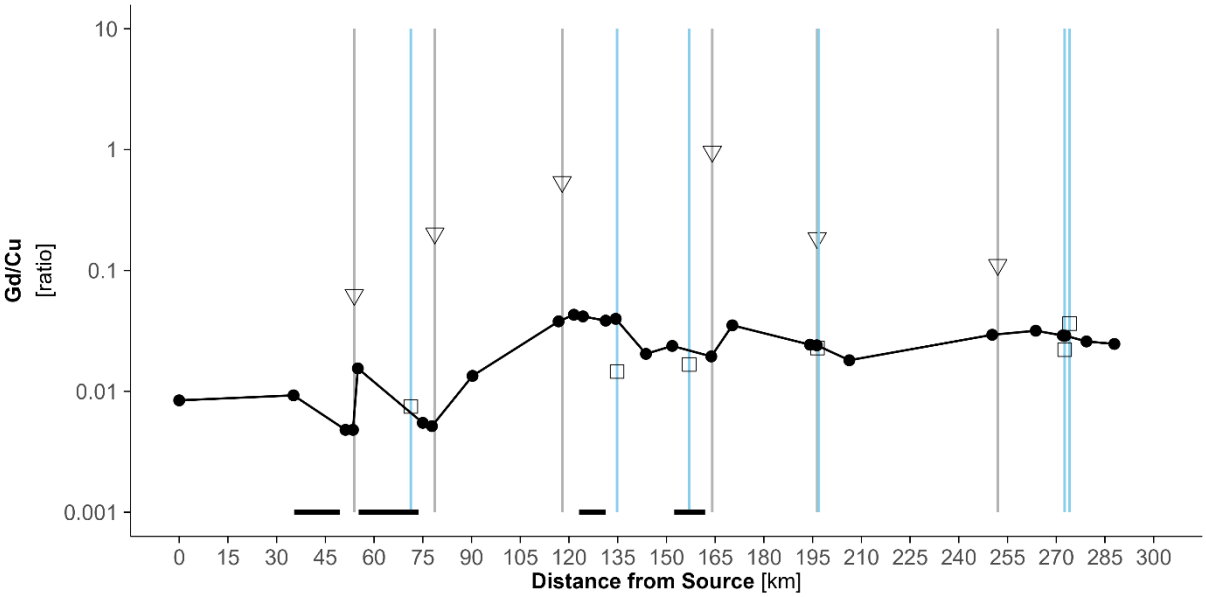

Figure S4: Gd/Cu ratios along the Aare River. Continuous black lines represent the ratio of Gd/Cu concentrations in river water along the river course, as an indicator of relative impact of healthcare-related activities. Triangles on grey bars indicate ratios in WWTP effluents, and squares on blue bars show ratios in the inputs from tributaries. Flow-through lakes are shown as black bars on the x-axis: 1) Brienzersee, 2) Thunersee, 3) Wohlensee, and 4) Bielersee. Major tributaries and corresponding WWTPs are labled on top.

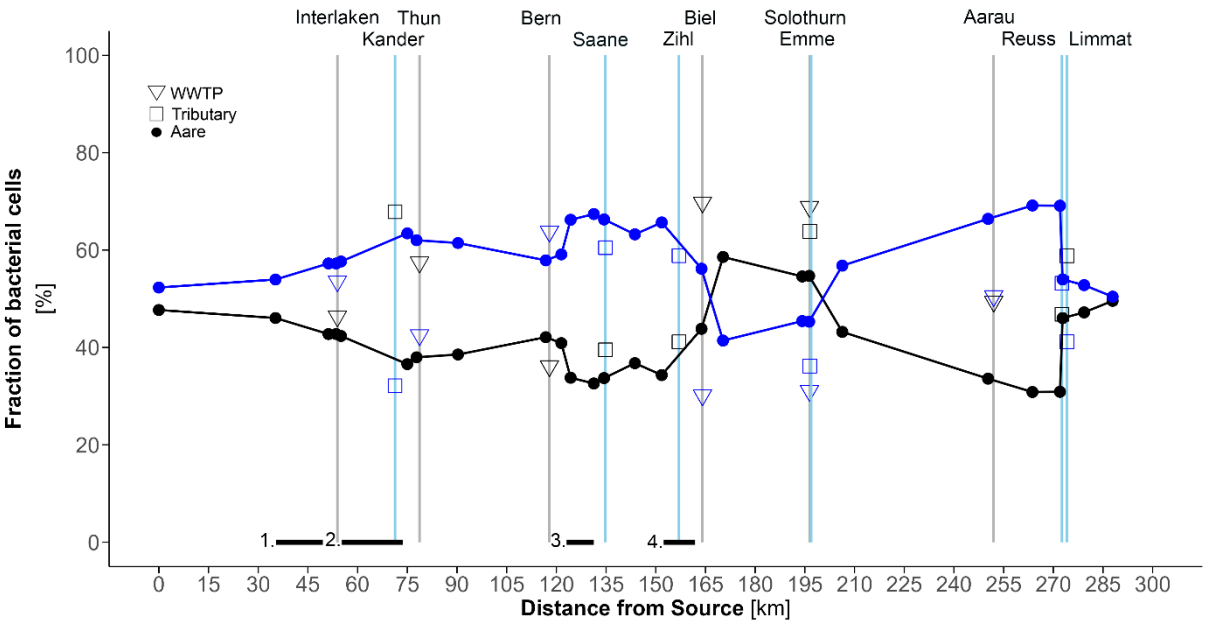

Figure S5: Percentage of bacterial cells with low and high nucleic acid (LNA and HNA) content along the Aare River. Fractions of LNA and HNA cells are shown along the river course (LNA: black and HNA: blue lines), in WWTP effluents (triangles on grey bars), and in tributaries (squares on blue bars). Flow-through lakes are indicated as black bars on the x-axis: 1) Brienzersee, 2) Thunersee, 3) Wohlensee, and 4) Bielersee. Raw data is provided in **Table S1**.

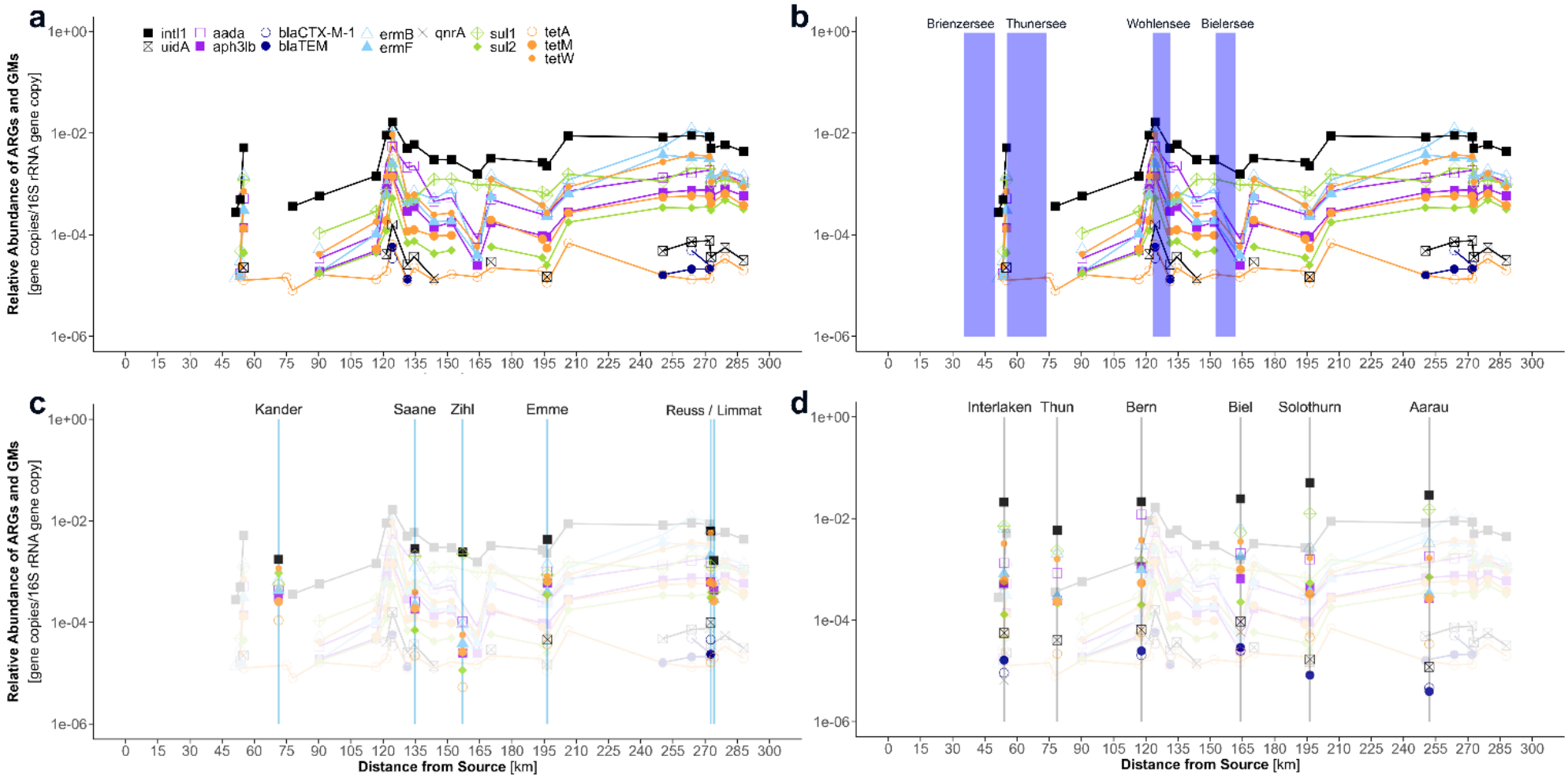

Figure S6*:* Relative abundance (gene copies/16S rRNA gene copy) of ARGs and GMs, quantified using qPCR. The concentration trends in the Aare River (a) are shown as line plots, while the abundance measured in (c) tributary inflows and (d) WWTP effluents is depicted as symbols within the bars (tributaries: blue / WWTP: gray). Flow-through lakes are indicated as bars in (b). Raw data is provided in **Table S1**.

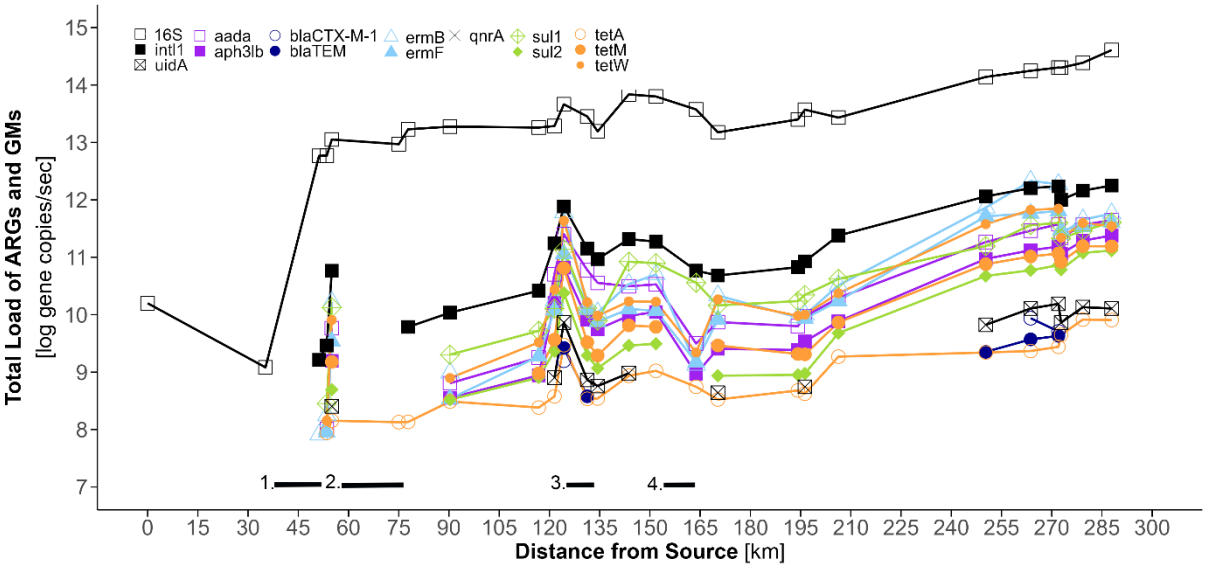

Figure S7: Calculated total ARG and GM load along Aare River. Line plots show log10-transformed mean discharge rates of ARGs and GM, normalized to river discharge. Discharge data from gauging stations along the main course and tributary inflows were used as the basis for a simple interpolation model to calculate discharge at each sampling point (see **Table S12, S13**). ARG and discharge data were then used to calculate total loads (**eq. 3**). Flow-through lakes are indicated as black bars on the x-axis: 1) Brienzersee, 2) Thunersee, 3) Wohlensee, and 4) Bielersee.

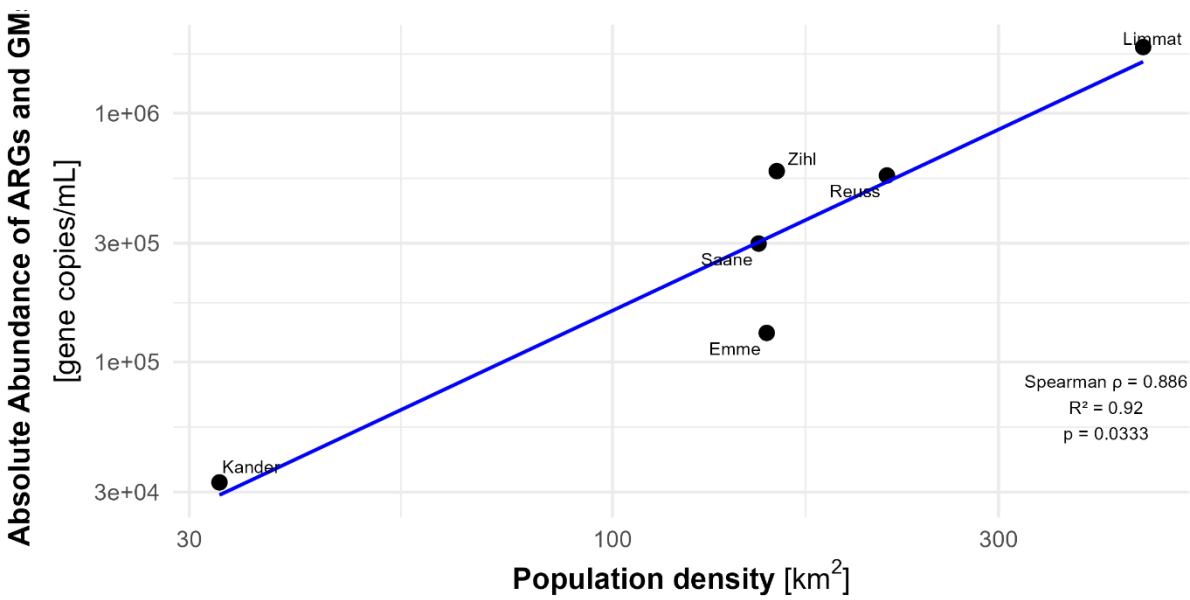

Figure S8: Positive association between catchment population density and the summed up abundance of ARG and GM in Aare River tributaries. Population density refers to inhabitants per km² of each tributary. The blue line shows the fitted linear regression ($R^2 = 0.92$, $p = 0.0333$), indicating a strong correlation (Spearman $\rho = 0.886$) between the sum of ARG and GM abundances and population density in the tributaries' catchment.

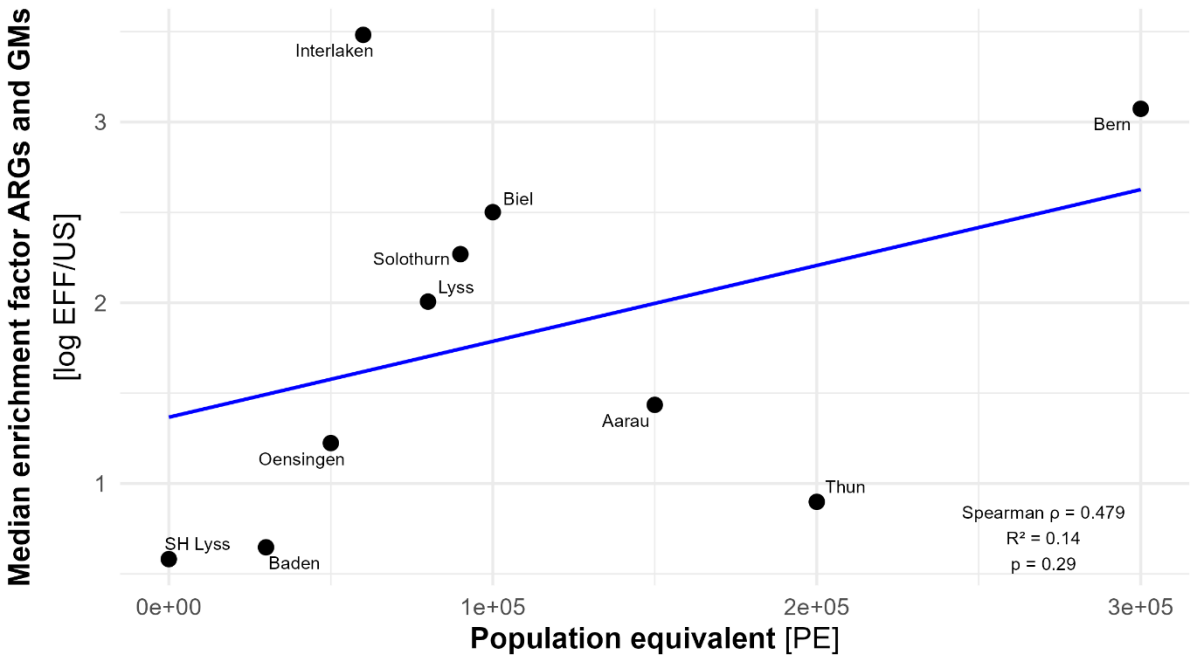

Figure S9: Relationship between median enrichment of ARGs and GMs and design capacity of WWTPs (population equicvalents). Each point represents one WWTP, labeled by location. The blue line indicates linear regression fit ($R^2 = 0.14$), with corresponding Spearman's rank correlation ($\rho = 0.479$) and p-value ($p = 0.29$) on the plot. A positive but non-statistical significant trend suggests slightly higher enrichment of ARGs and GMs in effluent relative to the upstream river with increasing WWTP size.

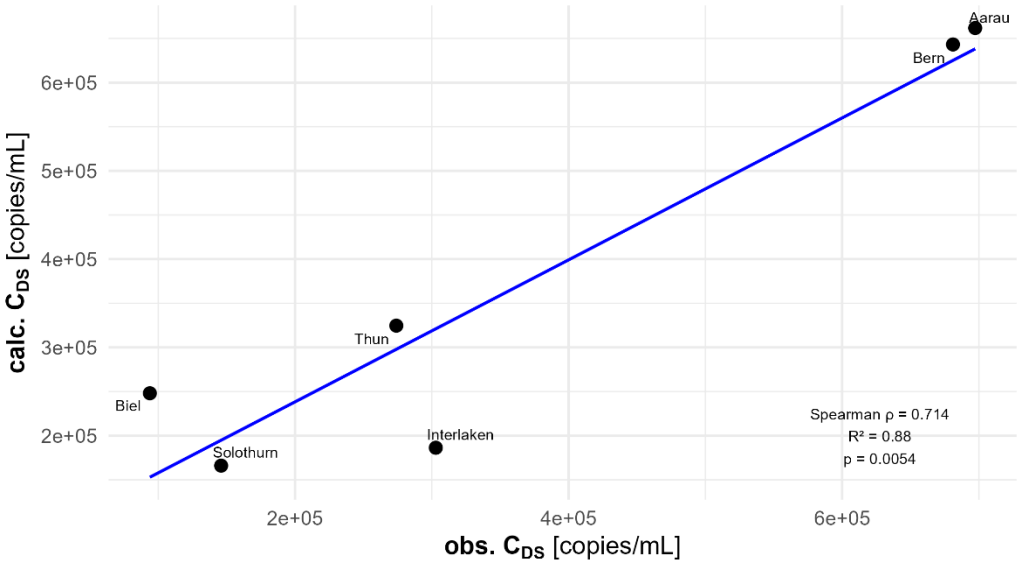

Figure S10: Relationship between calculated and observed downstream ARG concentrations in the Aare River. Calculated gene concentrations (calc. C_{DS}) derived from the discharge-based mixing model using measured WWTP and river flow data [m^3/s], by calculating $C_{DS} = (Q_{US\text{-}River} * C_{US\text{-}River} + Q_{WWTP} * C_{WWTP}) / (Q_{River} + Q_{WWTP})$. Observed values (obs. C_{DS}) represent the sum of gene concentrations measured downstream of the WWTP effluent inlet. A strong positive association was found between calc. C_{DS} and obs. C_{DS} concentrations (Spearman $\rho = 0.71$, $p = 0.14$), and the linear regression explained most of the variance (R2 = 0.88, $p = 0.005$, $y = 77'500 + 0.804 * x$). Together, these findings indicate that ARG levels downstream of WWTPs are closely linked to anthropogenic inputs from treated WW effluents.

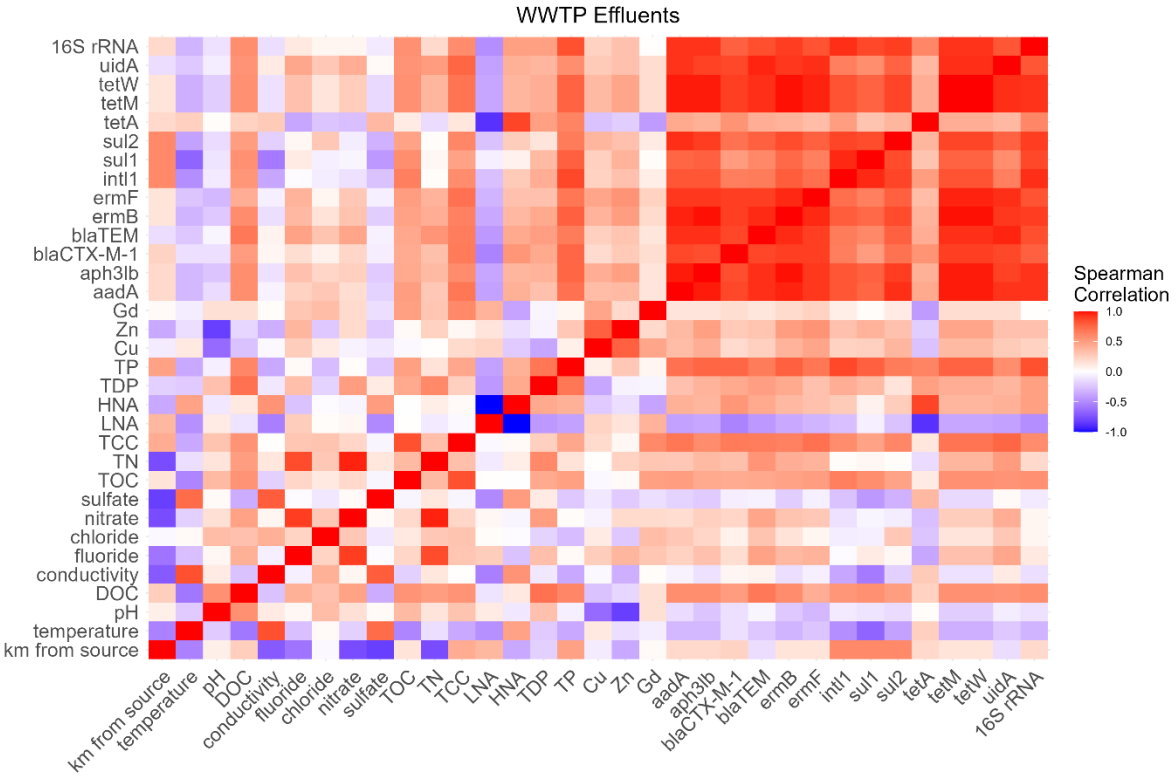

Figure S11: Heatmap of Spearman correlation matrix, including quantified genes, physicochemical parameters, and biological indicators between all WWTP effluent samples. Red: indicates positive correlation (ρ = 1), white: indicates no correlation (ρ = 0), blue: negative correlation (ρ= -1).

References

1. Rathinavelu, S., Beck, K., Wälchli, D. L. & Bürgmann, H. Optimization and validation of a consolidated Set of TaqMan qPCR assays for the surveillance of clinically relevant antibiotic resistance genes in environmental matrices. *MethodsX* **15,** 103600; 10.1016/j.mex.2025.103600 (2025).
2. McMurdie, P. J. & Holmes, S. phyloseq: an R package for reproducible interactive analysis and graphics of microbiome census data. *PloS one* **8,** e61217; 10.1371/journal.pone.0061217 (2013).
3. Janssen, D. J. *et al.* Biogeochemical cycling of trace elements and nutrients in ferruginous waters: Constraints from a deep oligotrophic ancient lake. *Limnology & Oceanography* **69,** 2775–2790; 10.1002/lno.12687 (2024).